2018

Novel Wideband EBG Structures For Isolation Improvement Between Cosite Antennas

Paul John Czeresko III
University of South Carolina

NOVEL WIDEBAND EBG STRUCTURES FOR ISOLATION IMPROVEMENT BETWEEN COSITE ANTENNAS

by

Paul John Czeresko III

Bachelor of Science
University of South Carolina, 2016

Submitted in Partial Fulfillment of the Requirements

For the Degree of Master of Science in

Electrical Engineering

College of Engineering and Computing

University of South Carolina

2018

Accepted by:

Mohammod Ali, Director of Thesis

Grigory Simin, Reader

Cheryl L. Addy, Vice Provost and Dean of the Graduate School

DEDICATION

I am dedicating my thesis and all its associated efforts to my grandfather, Stan Green. He instilled in me the inquisitive mind of a scientist from a young age and his library was invaluable to my early appreciation and understanding of the natural world.

ACKNOWLEDGEMENTS

I would like to thank Dr. Terry Vogler and The Boeing Company for supporting the work leading to this thesis. Their continued belief in and support of this project made this research possible.

I am also grateful to Dr. Mohammod Ali and the University of South Carolina for guiding and encouraging my education for the past five years.

ABSTRACT

As the number of installed antennas increases on a structure, the available real estate to do so without each antenna interfering with the others diminishes. Electromagnetic band gap (EBG) structures are one way to mitigate this cosite interference with compact antenna installations. While a host of EBG structures and types (3-D, planar etc.) have been proposed and studied historically, it has been found that planar EBG structures tend to provide very narrow bandwidths for both antenna design and cosite interference reduction. This research focuses on the design of EBG structures intended to achieve greater than 20 dB of isolation improvement in the 960-1220 MHz frequency band. Since the antenna bandwidth to be supported is quite substantial, our focus was to investigate the 3-D mushroom EBG structure or the so called Sievenpiper EBG structure [1].

In this research, many models and simulations including parametric optimization were performed to meet the isolation improvement goal across the desired frequency while maintaining return loss performance, radiation pattern, and gain. Focus was also placed in terms of the practicality of fabricating the EBG structure in terms of materials, size, and weight. And thus subsequently more practical approaches to traditional mushroom EBGs were developed that include EBG patches printed on very thin sheets of dielectric materials and are supported by thick foam substrates. Ultimately, the simulated results of an EBG design capable of improving isolation between blade antennas by at least 20 dB from 980-1240 MHz is presented. Efforts in developing an analytical model of such a structure based on lumped circuit elements is also discussed.

TABLE OF CONTENTS

Dedication iii

Acknowledgements iv

Abstract v

List of Tables viii

List of Figures ix

Chapter 1: Introduction 1

1.1 Motivation and Objectives 1

1.2 Outline of Thesis 2

Chapter 2: Preliminary Simulation Results 4

2.1 Wire Monopoles with Substrate on Entire Ground Plane 4

2.2 Wire Monopoles with Truncated TMM Substrate 8

2.3 Lightweight EBG Concept: EBG on Foam-like Substrate 10

Chapter 3: Broadband Monopoles with EBG 14

3.1 Broadband Antenna Design 14

3.2 Box Monopoles with Truncated EBG Substrate 14

3.3 Box Monopoles with EBG on Foam-like Substrate 16

3.4 Hybrid TMM and Foam Substrate 18

3.5 Multilayer EBGs 22

Chapter 4: Multilayer EBGs with Practical L-band Blade Antennas 27

Chapter 5: Multilayer EBG with Wideband Patch Antennas 40

Chapter 6: Analytical Model and Future Work 44

6.1 Analytical Model and Matlab Model 44

Chapter 7: Conclusions 51

7.1: EBG Efficacy for Retrofit Cosite Interference Reduction 51

7.2: Current State of Analytical Model 52

Chapter 8: Future Work 53

References 54

LIST OF TABLES

Table 2.1: Preliminary EBG parameters with 11.8 mm thick TMM4 substrate. 4

Table 2.2: EBG parameters for foam-like Substrate. 11

Table 3.1: Dimensions of broadband box monopole. 14

Table 4.1: Blade antenna VSWR specifications 27

Table 4.2: EBG dimensions for best-case with $Nz = 2$. 28

Table 4.3: Best case EBG dimensions for $Nz = 2$, $N = 9$. 29

Table 6.1: EBG parameters for first-order Matlab simulation 44

LIST OF FIGURES

Figure 2.1: Cosite monopole antennas with EBG structure – initial design. 5

Figure 2.2: S11 representing the geometry of Figure 2.1. 6

Figure 2.3: S21 representing the geometry of Figure 2.1. 6

Figure 2.4: Azimuthal radiation patterns for the geometry in Figure 2.1. 8

Figure 2.5: Two monopoles with EBG on truncated TMM.....9

Figure 2.6: Antenna S11 corresponding to the geometry of Figure 2.5. 9

Figure 2.7: S21 corresponding to the geometry of Figure 2.5. 10

Figure 2.8: Radiation pattern corresponding to the geometry of Figure 2.5.....10

Figure 2.9: Antenna S11 for low dielectric substrate ($\varepsilon_r = 1.2$). 12

Figure 2.10: S21 for low dielectric substrate ($\varepsilon_r = 1.2$). 12

Figure 2.11: Radiation patterns for low dielectric substrate ($\varepsilon_r = 1.2$). 13

Figure 3.1: Box monopoles with EBG on TMM. 15

Figure 3.2: S11 for box monopoles with EBG on TMM ($\varepsilon_r = 4.5$) and EBG dimensions as in Table 2.1. 16

Figure 3.3: S21 for box monopoles with EBG on TMM ($\varepsilon_r = 4.5$) and EBG dimensions as in Table 2.1. 17

Figure 3.4: S11 for foam substrate ($\varepsilon_r = 1.2$) with box monopoles. 18

Figure 3.5: S21 for foam substrate ($\varepsilon_r = 1.2$) with box monopoles. 18

Figure 3.6: Cross section of hybrid substrate (not to scale) - ε_1 represents foam of thickness 0.5 mm, ε_2 represents TMM4 of thickness 14.5 mm. 19

Figure 3.7: HFSS model of box monopoles with the hybrid substrate of Figure 3.6 with EBG dimensions as in Table 2.2. 19

Figure 3.8: S11 for hybrid substrate of Figure 3.6 with EBG dimensions as in Table 2.2. 20

Figure 3.9: S21 for hybrid substrate of Figure 3.6 with EBG dimensions as in Table 2.2. 21

Figure 3.10: Antenna S11 for increased values of *N* on hybrid substrate of Figure 3.6 with EBG dimensions as in Table 2.2. 21

Figure 3.11: S21 for increased values of *N* on hybrid substrate of Figure 3.6 with EBG dimensions as in Table 2.2. 22

Figure 3.12: Cross section of EBG stackup. 23

Figure 3.13: S11 for single-layer and two-layer EBG stackups – *N* = 9 and EBG dimensions as in Table 2.2. 24

Figure 3.14: S21 for single-layer and two-layer EBG stackups – *N* = 9 and EBG dimensions as in Table 2.2 25

Figure 3.15: S11 for single-layer and two-layer EBG stackups – *N* = 11 and EBG dimensions as in Table 2.2 25

Figure 3.16: S21 for single-layer and two-layer EBG stackups – *N* = 11 and EBG dimensions as in Table 2.2. 26

Figure 4.1: Blade antenna 3-D view in HFSS (ground plane size for illustration only). 27

Figure 4.2: VSWR for structure in Figure 4.1 with markers indicating design bounds given in datasheet. 28

Figure 4.3: Best S21 cases for big sweep with blade antennas – *N* = 9 with EBG dimensions as in Table 2.2. 29

Figure 4.4: S21 for 32, 35, and 40 mm patch width – all other design parameters the same as previous case. 30

Figure 4.5: S11 for 32, 35, and 40 mm patch width – all other design parameters the same as previous case. 30

Figure 4.6: S11 behavior for lower *N* values – EBG dimensions as in Table 4.3. 31

Figure 4.7: S21 behavior for lower *N* values – EBG dimensions as in Table 4.3 32

Figure 4.8: S11 results for parametric sweep of EBG dimensions fixing *N* = 5 and *Nz* = 3. 32

Figure 4.9: S21 results for parametric sweep of EBG dimensions fixing N = 5 and Nz = 3. 34

Figure 4.10: S21 results for g variation only, fixing w = 30 mm, h = 14.5 mm. 35

Figure 4.11: S21 results for w variation only, fixing g = 2 mm, h = 14.5 mm. 37

Figure 4.12: S21 results for h variation only, fixing w = 30 mm, g = 2 mm. 37

Figure 4.13: Comparison of best-case S21 results for previous Nz = 2, N = 5 structure and more compact Nz = 3, N = 5 structure.....38

Figure 4.14: Comparison of best-case S11 results for previous Nz = 2, N = 5 structure and more compact Nz = 3, N = 5 structure.....38

Figure 4.15: Radiation patterns at 1100 MHz for N = 5, Nz = 3 39

Figure 5.1: Aperture coupled patches with EBGs as seen in HFSS. 41

Figure 5.2: Simulated S11 as function of number of EBG columns in between two aperture coupled patches (antenna edge-to-edge distance=268 mm). 41

Figure 5.3: Simulated S21 as function of number of EBG columns in between two aperture coupled patches (antenna edge-to-edge distance=268 mm). 42

Figure 5.4: Simulated S11 as function of EBG parameters by varying w from 30 to 40 mm at 1 mm increments and g from 1.6 to 2.6 mm at 0.1 mm increments (antenna edge-to-edge distance=384 mm). 43

Figure 5.5: Greater than 30 dB coupling reduction shown for L2 in best case. 43

Figure 6.1: High-level schematic of first order lumped circuit model of EBG structure.....45

Figure 6.2: S-parameter plots for initial EBG analysis in Matlab. 46

Figure 6.3: Electric field magnitude on EBG patches of the dimensions in Table 6.1.....47

Figure 6.4: Illustration of E-field probes along patch edges (top view). 48

Figure 6.5: Illustration of surface current probe along via length (side view). 48

Figure 6.6: Normalized gap capacitance coefficients. 49

Figure 6.7: Normalized via inductance coefficients. 49

Figure 6.8: S-parameter output for Matlab model with modified scaling factors. 50

CHAPTER 1: INTRODUCTION

1.1 MOTIVATION AND OBJECTIVES

The objective of this research was to study and design EBG structures to significantly reduce or suppress the mutual coupling between vertical monopole antennas with typically omnidirectional patterns. Such monopole antennas are used on aircraft for communication and other applications. Specific frequency band of interest was the L-band (960-1220 MHz). In the literature, EBG structures have been designed and proposed to develop thin, low profile dipole, spiral, and bow-ties antennas [1-18]. They have also been proposed to reduce or suppress the mutual coupling between antennas [19-24]. A large number of articles have been written on coupling reduction between patch antennas for array development. Naturally, the focus has been to utilize the whole substrate of the array and develop the EBG as an integral part of that substrate. With such design approaches the antenna development effort and the EBG design effort are coupled. This thesis reports research focused on studying and developing EBG structures for cosite interference reduction with the fact remaining that any antenna design efforts were not an integral part of the EBG design or its functionality. In that respect, this effort could be termed a retrofit approach in that the resulting EBG structures could be placed as an add-on to existing antenna platforms without significantly affecting the antenna properties, e.g. return loss bandwidth, radiation pattern coverage and gain. As this work progressed, it became apparent that a significantly simpler case study should be considered to understand the role each design parameter played in the overall behavior of the structure. For this reason, a

simplified model was developed, the goal and purpose of which was to be able to describe and predict its behavior analytically.

1.2 Outline of Thesis

The first chapter of the thesis provides an explanation of the motivation for this work and a brief review of existing efforts and literature on the topic. Chapter 2 describes a preliminary effort to apply previous EBG designs to the context under investigation. In this second chapter, an EBG structure designed by our group earlier is scaled and placed between two wire monopole antennas in an Ansys HFSS simulation environment. Various substrate configurations are investigated and the resulting S-parameter and radiation pattern data are reported. The third chapter discusses a broadband monopole antenna and the resulting behavior the EBG design up to that point displays. This chapter also introduces a hybrid material substrate and multilayer EBG structures for the purpose of compacting the design while simultaneously improving interference rejection performance. Chapter 4 covers the effort toward applying the insight gained in Chapter 3 to an example with practical antennas, namely L-band blades based on a common aviation antenna available in the market. The effect of each of the EBG design parameters on overall performance is investigated in greater depth and those conclusions are reported along with accompanying S-parameter and radiation pattern data. A similar effort is reported in Chapter 5, but this time applied to a wideband patch antenna covering the L1 and L2 GPS bands. A viable solution set is obtained and reported. Chapter 6 discusses an analytical model of a simplified form of the EBG structure designed thus far, in order to better understand the underlying concepts that drive the efficacy of any given design configuration. This model is based on lumped circuit elements and is expressed

numerically in Matlab. Although this work is very preliminary, the approach and results so far are discussed. Chapter 7 presents the conclusions made based on all the work presented and Chapter 8 discusses areas of future development.

CHAPTER 2: PRELIMINARY SIMULATION RESULTS

2.1 WIRE MONOPOLES WITH SUBSTRATE ON ENTIRE GROUND PLANE

To examine the efficacy of a mushroom-EBG structure in coupling reduction between two L-band antennas, a simple model was constructed in HFSS where an EBG structure was placed between two monopole antennas, shown in Figure 2.1. The dimensions of this initial EBG structure were obtained from the direct scaling (doubling) of an EBG structure designed by our group earlier [16]. Since the reference structure was designed using a TMM4 substrate, the same was used here also. In this configuration the TMM substrate occupies the complete structure and hence labeled "full sheet." In Figure 2.1 the grounded substrate measures 725 mm by 545 mm. The two monopole antennas are separated by a distance, d = 203 mm. The length and wire diameter of each monopole were 62.7 mm and 1.3 mm, respectively. As seen, there are three columns (denoted henceforth as N = 3) of EBG patches with a via placed at the center of each patch. The number of EBG patches and vias in one column is fixed at 10. The diameter of each via was 1 mm. Parametric sweeps were performed in HFSS to fine-tune the dimensions, resulting in the EBG parameters listed in Table 2.1

Table 2.1: Preliminary EBG parameters with 11.8 mm thick TMM4 substrate.

Design Parameter	Size (mm)
Height h	11.8
Width w	24.8
Gap g	0.8
Ant. spacing d	203

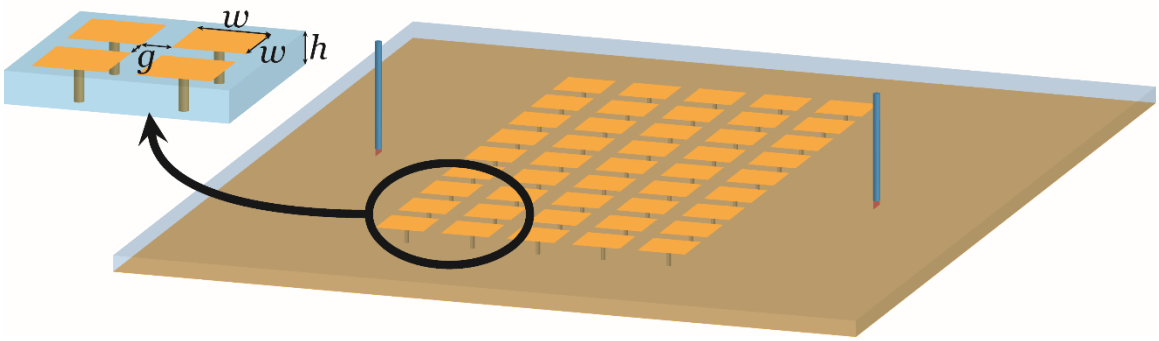

Figure 2.1: Cosite monopole antennas with EBG structure – initial design.

Simulated S11 and S21 plots are shown in Figure 2.2 and Figure 2.3, respectively. These results are obtained by varying the number of EBG columns, *N*, as 0, 1, 3, and 5, respectively between the monopole antennas. Thus, $N = 5$ means there are five EBG columns in between the monopoles or 5 times 10 EBG patches and vias. For $N = 5$, the distance between the edge of the nearest EBG patch and the monopole antenna is 70.4 mm or 0.2253λ, where λ is the free-space wavelength corresponding to the lowest operating frequency of interest here, e.g. 960 MHz. It is clear from Figure 2.2 that the present monopole antenna made from a thin cylindrical wire does not meet the L-band bandwidth requirement of 960-1220 MHz. For the case with no EBG, or $N = 0$, the antenna bandwidth is from 1040 to 1200 MHz. As seen from Figure 2.2, the presence of the EBG for any number of EBG columns has only negligible effect on the antenna S11 bandwidth (within -10 dB). There has been no frequency shift at the lower end of the band while the frequency at the upper end increased by 50 MHz.

Simulated coupling data between the two monopoles can be seen from Figure 2.3. Clearly the presence of the EBG creates a resonance effect that resembles the behavior of a stop-band filter. For example, for $N = 1$ there is a sharp reduction in coupling at around 990 MHz (60 MHz ahead of the antenna resonance). There is about 23 dB of coupling reduction observed at 990 MHz albeit within an extremely narrow frequency range, just a

few MHz. For N = 3 and N = 5 the frequencies at which maximum coupling reduction is observed are 1110 and 1175 MHz, respectively.

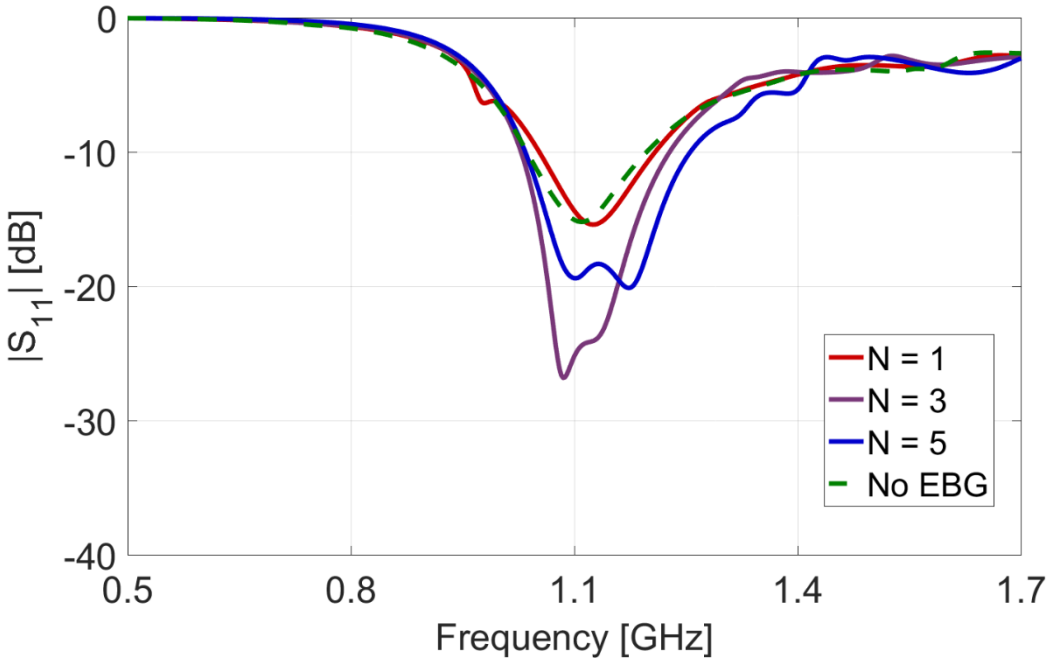

Figure 2.2: S11 representing the geometry of Figure 2.1.

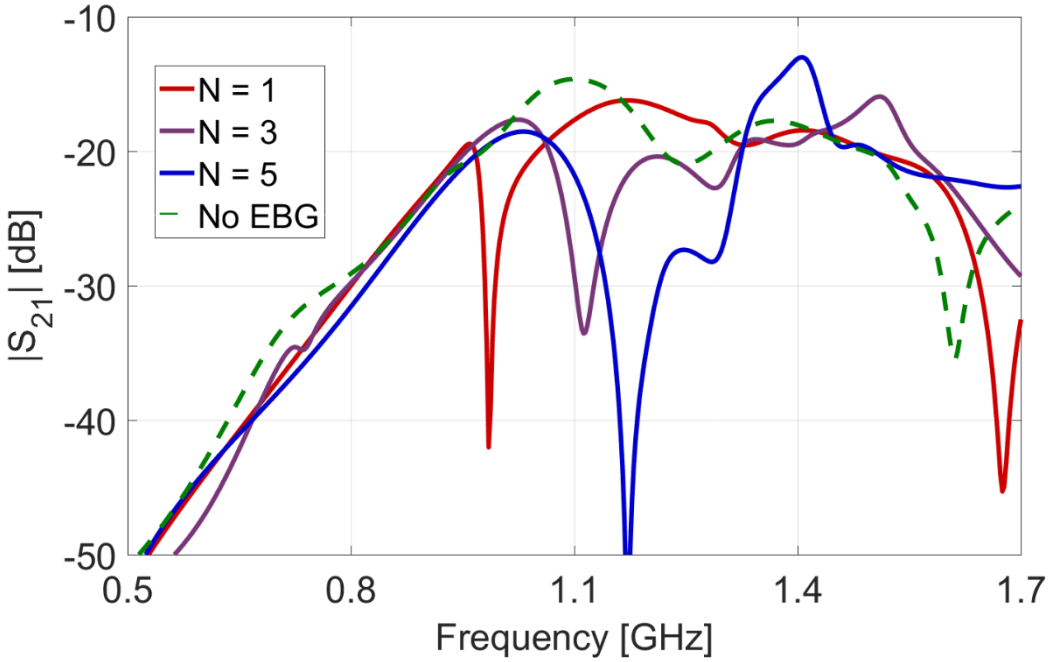

Figure 2.3: S21 representing the geometry of Figure 2.1.

Using the following equations yields a stopband frequency of 1033 MHz for the EBG.

$$L = \mu h \qquad (1)$$

$$C = \frac{w(\varepsilon_1 + \varepsilon_2)}{\pi} \cosh^{-1}\left[\frac{w+g}{g}\right] \qquad (2)$$

$$f = \frac{1}{2\pi\sqrt{L\,C}} \qquad (3)$$

The differences observed among the three frequencies e.g., 990, 1110, and 1175 MHz can be understood from the fact that the EBG is in the near field of the monopoles. As *N* increases the EBG gets closer and closer to the monopole's near field. If the monopoles are placed at least 0.5λ away from the nearest EBG patch for the largest *N* the differences in S21 responses between various *N* should decrease.

It is clear that with an increase in the number of EBG columns two things are observed, the bandwidth of coupling reduction increases and the frequency shifts higher. The bandwidth in coupling reduction is fairly intuitive because if the number of stages is increased the stop-band bandwidth is expected to increase. Explaining the latter is more complex and may require understanding the roles of all of the EBG parameters in terms of antenna-to-antenna coupling. Nevertheless, for $N = 5$ tremendous amount of coupling reduction (nearly 38 dB) is observed at 1175 MHz, which is still within the operating frequency band of the antenna; however, the frequency range within which at least 20 dB coupling reduction is obtained is very small (about 20 MHz) while the frequency range within which at least 10 dB coupling reduction is obtained is about 50 MHz. These numbers should be kept in perspective because our 20 dB coupling reduction goal is 260 MHz or nearly 24%.

Simulated azimuthal radiation patterns in the presence of the EBG are shown in Figure 2.4. To avoid an array pattern only source for one antenna was assigned an

excitation voltage. Note that even with $N = 0$ the pattern does show some non-uniformity or ripples primarily due to the small size of the ground plane and the presence of the thick TMM4 substrate. For other values of N the patterns show variations as well.

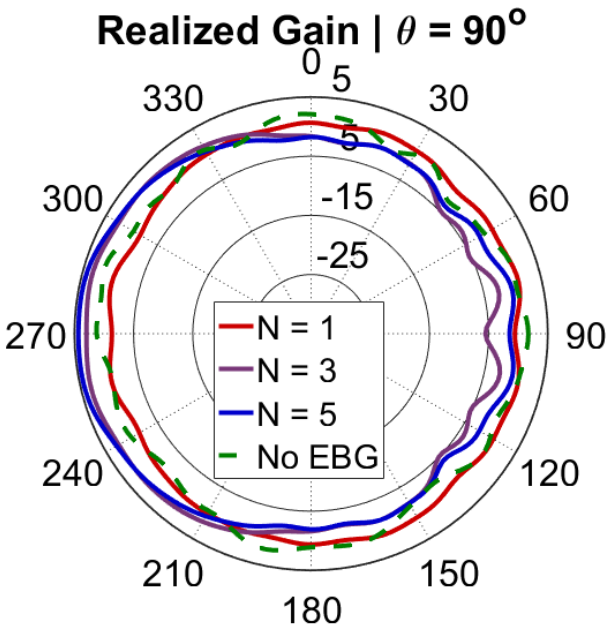

Figure 2.4: Azimuthal radiation patterns for the geometry in Figure 2.1.

2.2 Wire Monopoles with Truncated TMM Substrate

With retrofit as a goal, EBG structures on a truncated TMM substrate were simulated as shown in Figure 2.5. The dimensions were otherwise identical to the previous case. Simulated S11 and S21 data for this case are shown in Figure 2.6 and Figure 2.7, respectively. The S11 results are similar as before. The S21 response shows that coupling is reduced at 990, 1120, and 1175 MHz for $N = 1$, 3, and 5 respectively. The frequencies of maximum coupling reduction remained nearly unchanged with the amount of coupling reduction substantially lower than before. For example, for $N = 5$ the highest amount of coupling reduced is about 20 dB at 1175 MHz. Nevertheless, it is clear that having an EBG structure on a truncated substrate that can be designed and built completely separate from

the antenna does reduce the antenna to antenna coupling. Radiation patterns in Figure 2.8 show a slight reflection away from the EBG structure as seen before, but again maintain shape and are even less perturbed than the first case. For example, the azimuthal patterns show about 5 dB variation for $N = 3$.

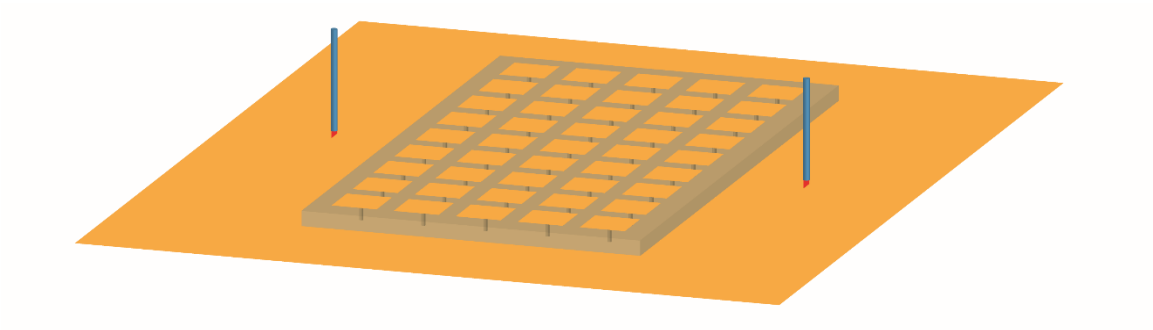

Figure 2.5: Two monopoles with EBG on truncated TMM.

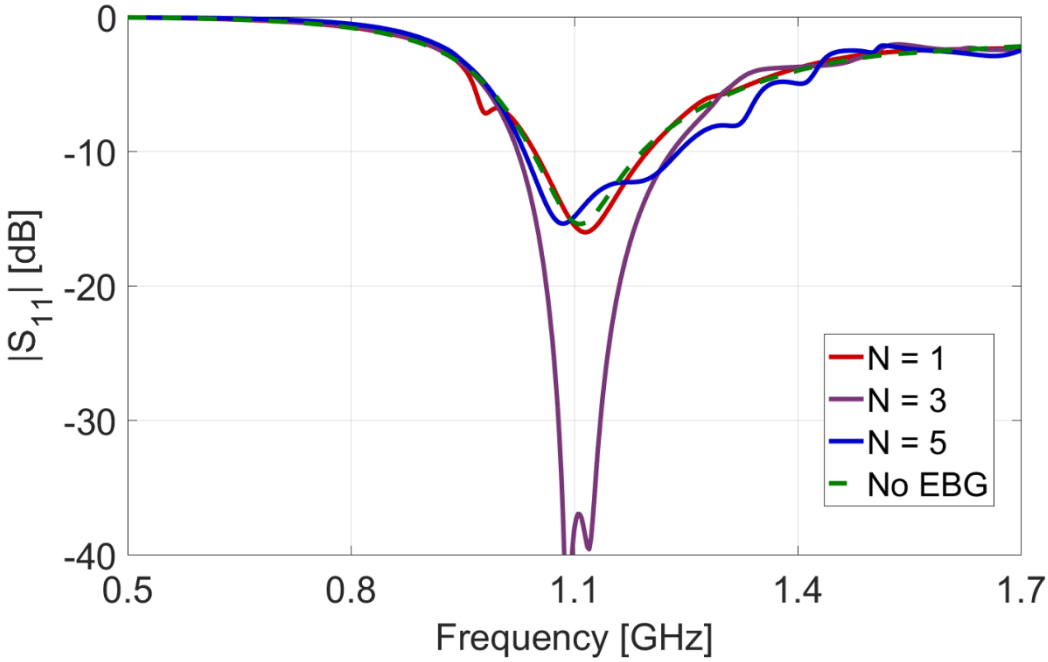

Figure 2.6: Antenna S11 corresponding to the geometry of Figure 2.5.

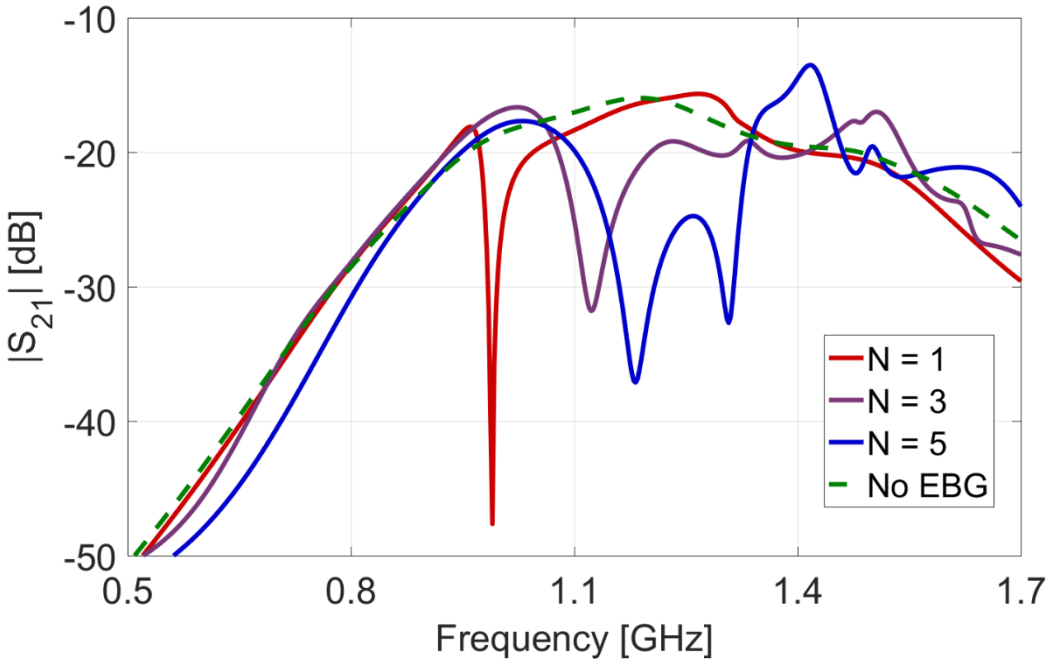

Figure 2.7: S21 corresponding to the geometry of Figure 2.5.

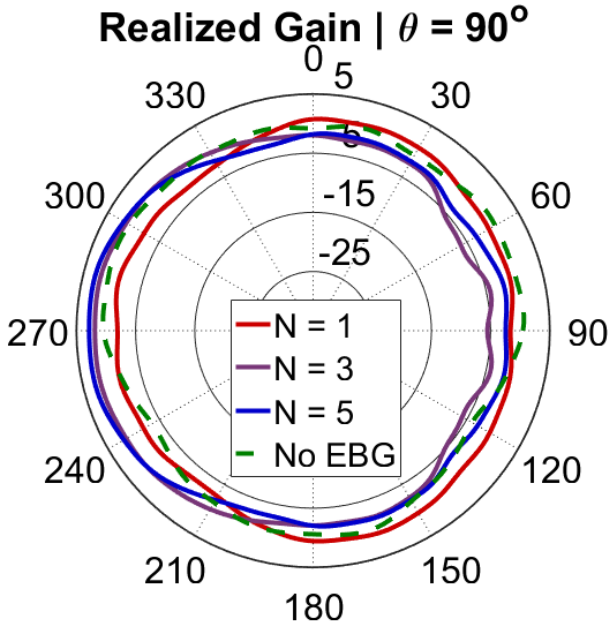

Figure 2.8: Radiation pattern corresponding to the geometry of Figure 2.5.

2.3 LIGHTWEIGHT EBG CONCEPT: EBG ON FOAM-LIKE SUBSTRATE

Since TMM4 is a relatively dense, heavy material, a lighter low-dielectric constant substrate was considered. Such a material was represented in HFSS as a "foam-like"

material with dielectric constant of $\varepsilon_r = 1.2$. This meant the EBG unit cell size had to be redesigned to maintain the same operating frequency. This resulted in the dimensions shown in Table 2.2.

Table 2.2: EBG parameters for foam-like Substrate.

Design Parameter	Size (mm)
Height h	15
Width w	44
Gap w	1.6
Ant. spacing d	203

Simulated S11 and S21 results with the low dielectric constant foam like substrate (truncated) are shown in Figure 2.9 and Figure 2.10, respectively. Results only for $N = 0$ and $N = 3$ are shown. There is a clear 50 MHz down-shift on the lower end of the S11 when the EBG is installed. The low dielectric constant material seemed to have widened the coupling reduction bandwidth at the cost of S21 depth. Within the antenna operating bandwidth, 1 to 1.15 GHz, the reduction in coupling is between 7 and 13 dB. The azimuthal patterns in Figure 2.11 show similar behavior as before.

Using equations (1)-(3) the obtain stopband frequency to be 1103 MHz considering the EBG parameters listed in Table 2.2.

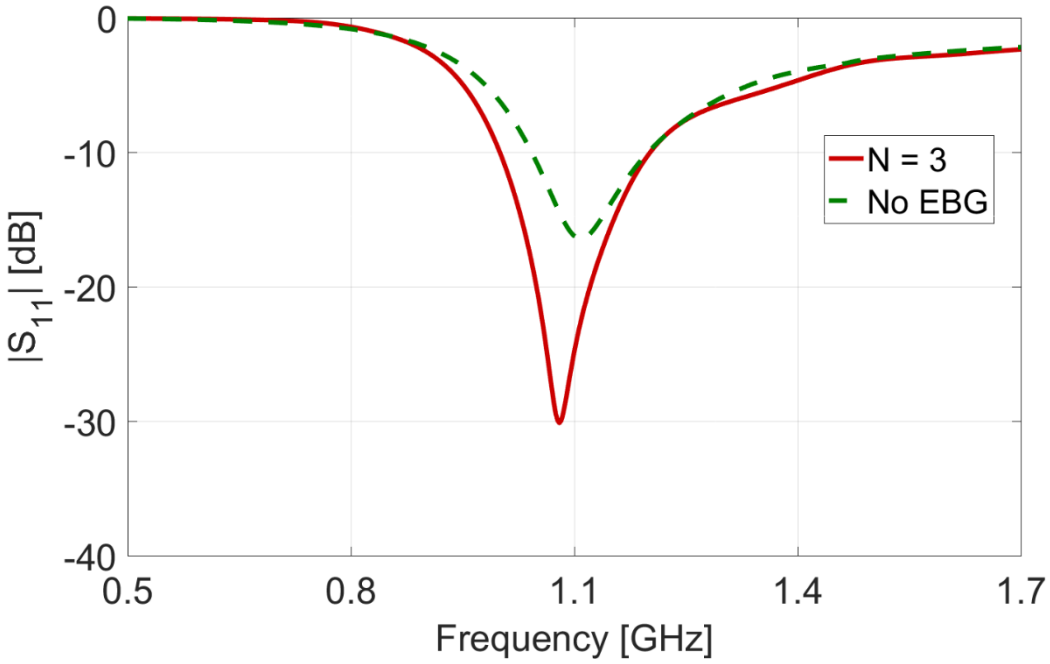

Figure 2.9: Antenna S11 for low dielectric substrate ($\varepsilon_r = 1.2$).

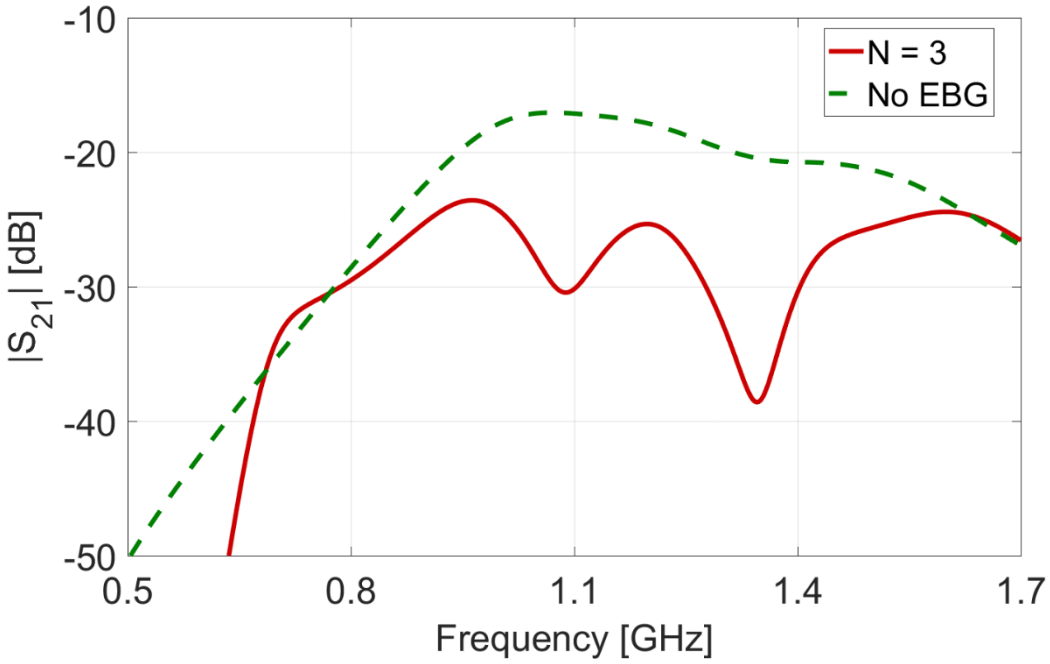

Figure 2.10: S21 for low dielectric substrate ($\varepsilon_r = 1.2$).

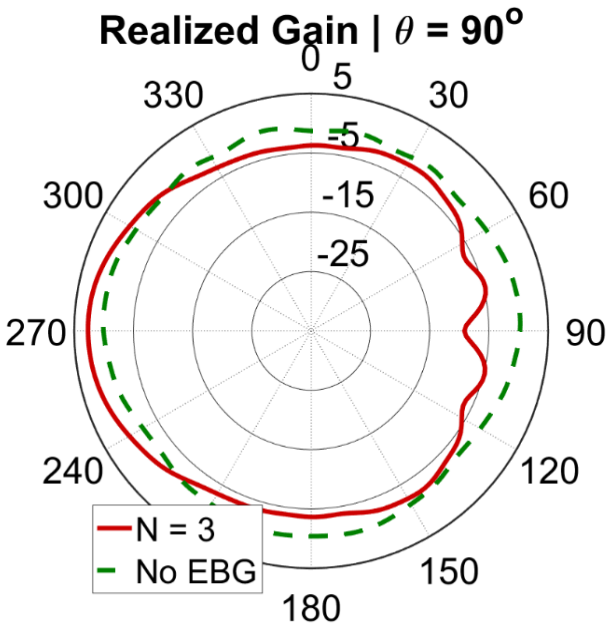

Figure 2.11: Radiation patterns for low dielectric substrate ($\varepsilon_r = 1.2$).

CHAPTER 3: BROADBAND MONOPOLES WITH EBG

3.1 BROADBAND ANTENNA DESIGN

The quarter-wave wire monopole used up to this point was too narrowband to reveal the full behavior of the EBG. For this reason, two box monopoles were designed in HFSS. These antennas consisted of a copper box with dimensions given in Table 3.1.

Table 3.1: Dimensions of broadband box monopole.

Dimension	Size (mm)
Height (in *z*)	62
Width (in *x*)	40
depth (in *y*)	20

These antennas provided a -10 dB S11 bandwidth from 760 MHz to 1500 MHz, or nearly an octave (2:1 frequency ratio). This is over three times the bandwidth of the wire monopoles and is more than sufficient to observe the entire design bandwidth with about 200 MHz of buffer on either end.

3.2 BOX MONOPOLES WITH TRUNCATED EBG SUBSTRATE

The configuration studied is shown in Figure 3.1 where the EBG structure was created on a piece of truncated TMM substrate ($\varepsilon_r = 4.5$). The antennas were spaced by a distance of d = 450 mm between feed to feed to allow for the inclusion of additional EBG columns. The EBG parameters were identical to Table 2.1: w = 24.8 mm, h = 11.8 mm, and g = 0.8 mm. Simulated S11 and S21 results for N = 0, 3, 5, 7, 13 are shown plotted in Figure 3.2 and Figure 3.3. The S11 results clearly show that the antenna operating frequency shifts higher with the EBG. For most of the cases a frequency increase of 50

MHz is observed at the low end except for N = 13 for which nearly 140 MHz of upward frequency shift at the low end is observed. The upward shift is likely due to the capacitive loading effects of the

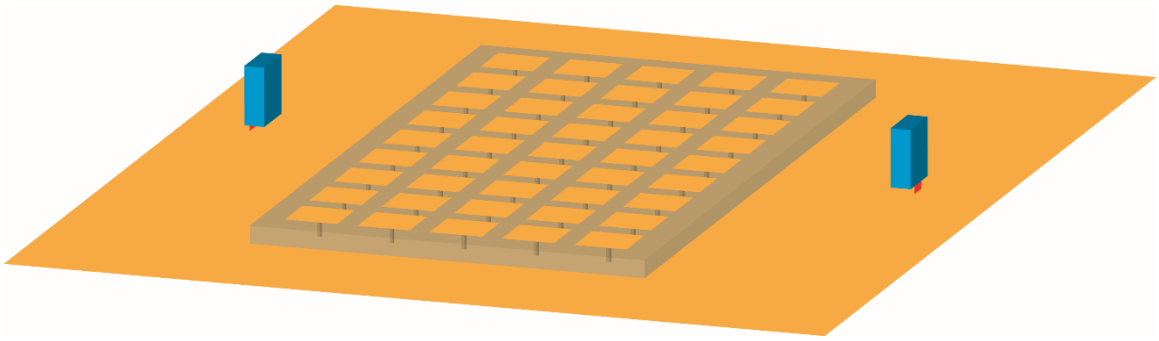

Figure 3.1: Box monopoles with EBG on TMM.

nearby EBG patches on the monopole antenna. Nevertheless, it is clear that since the frequency bandwidth is large with a broadband monopole, it is much easier to satisfy the required 960-1220 MHz of required bandwidth.

Since for all N the antenna easily satisfies the 960-1220 MHz of return loss bandwidth we will examine the S21 behavior due to EBGs within that frequency range. It is clear from the S21 plots in Figure 3.3 that the stopband of the EBG in general lies within 1100-1400 MHz. With increasing N the mutual coupling between the two antennas generally decreases. Maximum coupling reduction for N = 3, 5, 7, 13 are 23.1, 13.1, 22, and 26.4 dB that occurs at 1320, 1360, 1230, and 1300 MHz, respectively. In terms of coupling reduction bandwidth more reduction bandwidth is observed with greater N. For example, for N = 13 the coupling reduction bandwidth is from 1150-1340 MHz which is nearly 200 MHz where the mutual coupling is reduced between 9 dB to 30 dB. However, this band is largely outside the band of interest except for a small sliver at 1150-1220 MHz.

This indicates coupling reduction over a broader bandwidth is possible but would require significant optimization to address two challenges: (1) obtain > 20 dB coupling

reduction over the entire band and (2) have minimal to no effect on antenna return loss performance over the operating frequency band.

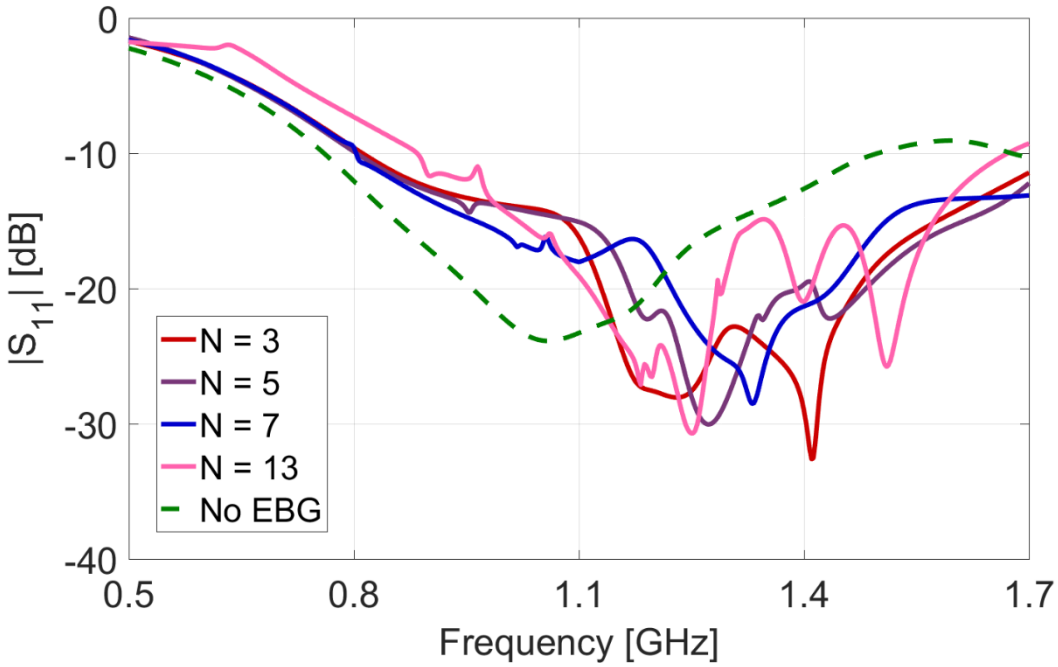

Figure 3.2: S11 for box monopoles with EBG on TMM ($\varepsilon_r = 4.5$) and EBG dimensions as in Table 2.1.

3.3 Box Monopoles with EBG on Foam-like Substrate

This same configuration was used for the foam-based EBG structure seen previously. The antennas were spaced by a distance of *d* = 450 mm. The EBG parameters identical to those in Table 2.2, but with an antenna spacing, *d*, of 450 mm. since the patch dimensions are much larger only up to *N* = 7 was considered.

Simulated S11 results shown in Figure 3.4 clearly show again an upward shift in the antenna operating frequency by about 50 MHz except for *N* = 5. The S21 in Figure 3.5 shows the lower intensity, wider bandwidth behavior compared to the TMM case. The foam case displays some rejection across most of the band, but no deep valleys. For

example, 6-15 dB coupling reduction is easily obtained throughout the band from 750-1500 MHz; that is a 2:1 frequency ratio.

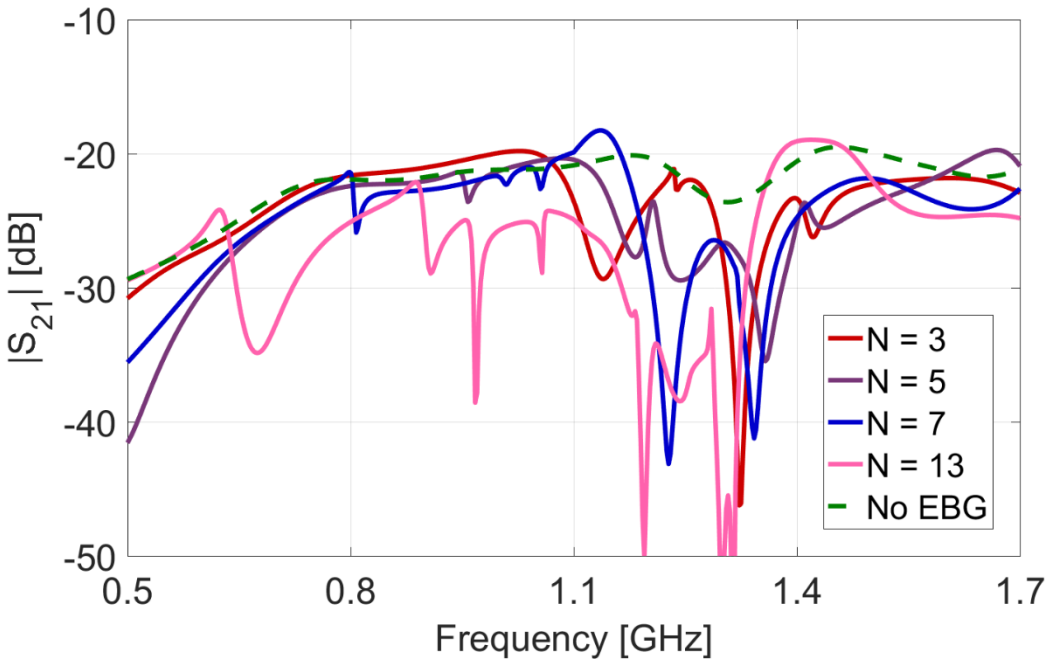

Figure 3.3: S21 for box monopoles with EBG on TMM ($\varepsilon_r = 4.5$) and EBG dimensions as in Table 2.1.

It is apparent that for broadband rejection a low dielectric constant material is a good choice. At the same time, comparing Figure 3.3 to Figure 3.5 it can be concluded that the amount of the coupling reduction over a certain band is higher with a higher dielectric constant material. These results prompted us to investigate a somewhat hybrid structure that can be comprised of a thin sheet of TMM supported by a thick piece of foam. If the hybrid substrate is successful in coupling reduction it will also lead to weight reduction. Since the edge-to-edge capacitance between the patches get affected by the dielectric material of the substrate this proposition has validity in it. We anticipate that the patch dimensions would have to increase from the TMM case for such a design.

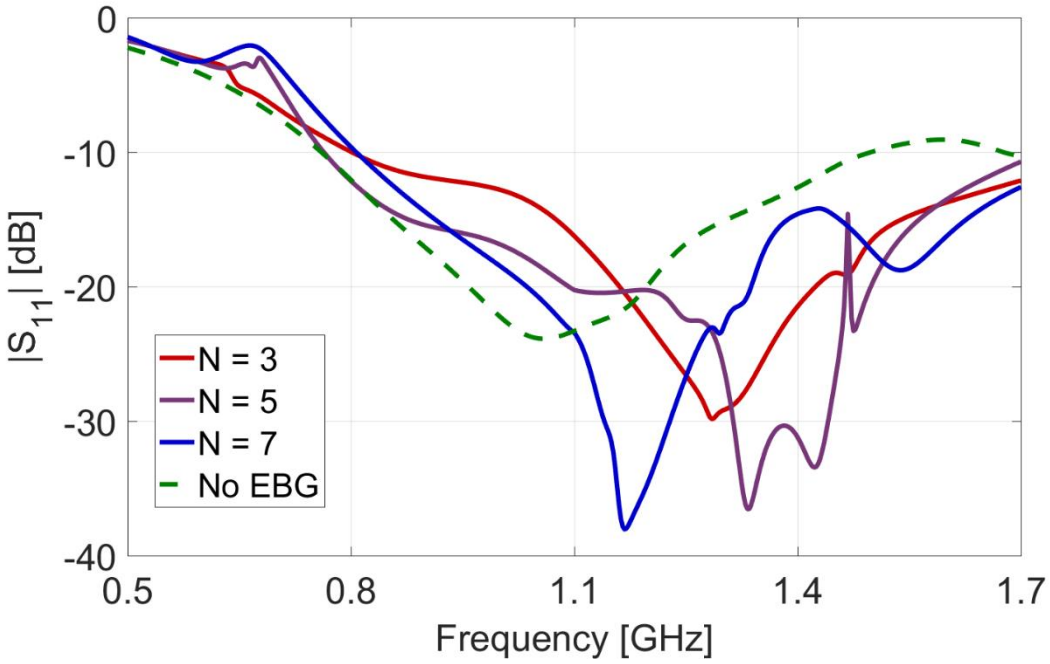

Figure 3.4: S11 for foam substrate ($\varepsilon_r = 1.2$) with box monopoles.

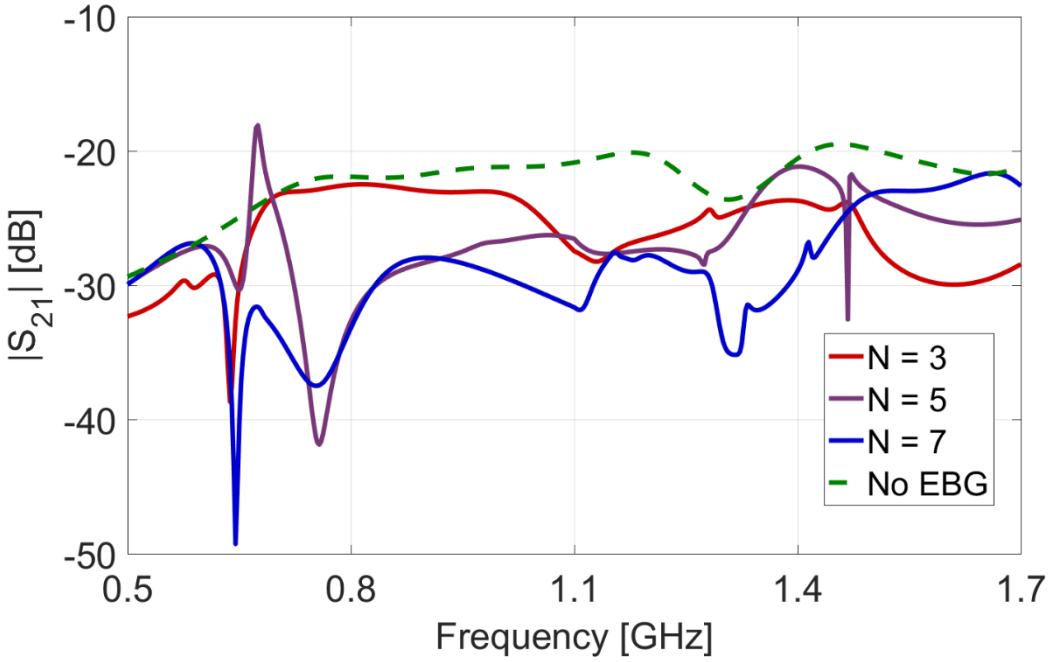

Figure 3.5: S21 for foam substrate ($\varepsilon_r = 1.2$) with box monopoles.

3.4 Hybrid TMM and Foam Substrate

Both the TMM and foam substrates exhibited certain desirable characteristics. The TMM had significant coupling reduction, but within a narrow bandwidth. The higher

dielectric constant also led to a physically smaller EBG structure. While the foam substrate provided a smoother rejection curve, the deepest magnitude of coupling reduction was only about half of what the TMM provided. The substrate material itself would be lighter in weight, but the patches and height must be larger than the TMM design to operate at the same frequency. Because of these reasons, a hybrid design was considered. This meant placing a thin sheet of TMM on top of a foam spacer, as illustrated in Figure 3.6 and Figure 3.7. In addition to the intention to exploit the attractive traits of each material, the practical application of such a design would allow patches of any size to be etched or printed onto very thin TMM then placed on top of foam, the thickness of which could achieve the proper height for inductance tuning. Below is a 2-D cross section of the described structure and a 3-D HFSS view.

Figure 3.6: Cross section of hybrid substrate (not to scale) - ε_1 represents foam of thickness 0.5 mm, ε_2 represents TMM4 of thickness 14.5 mm.

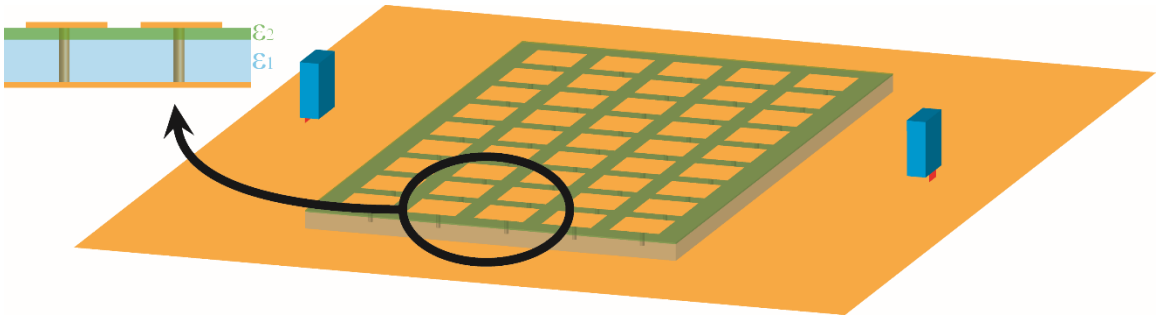

Figure 3.7: HFSS model of box monopoles with the hybrid substrate of Figure 3.6 with EBG dimensions as in Table 2.2.

As a first-order approximation, all the EBG design dimensions were kept the same as the bulk foam design shown in Table 2.2. The total substrate thickness was the same at 15 mm, comprised of a 0.5 mm sheet of TMM raised up by 14.5 mm of foam.

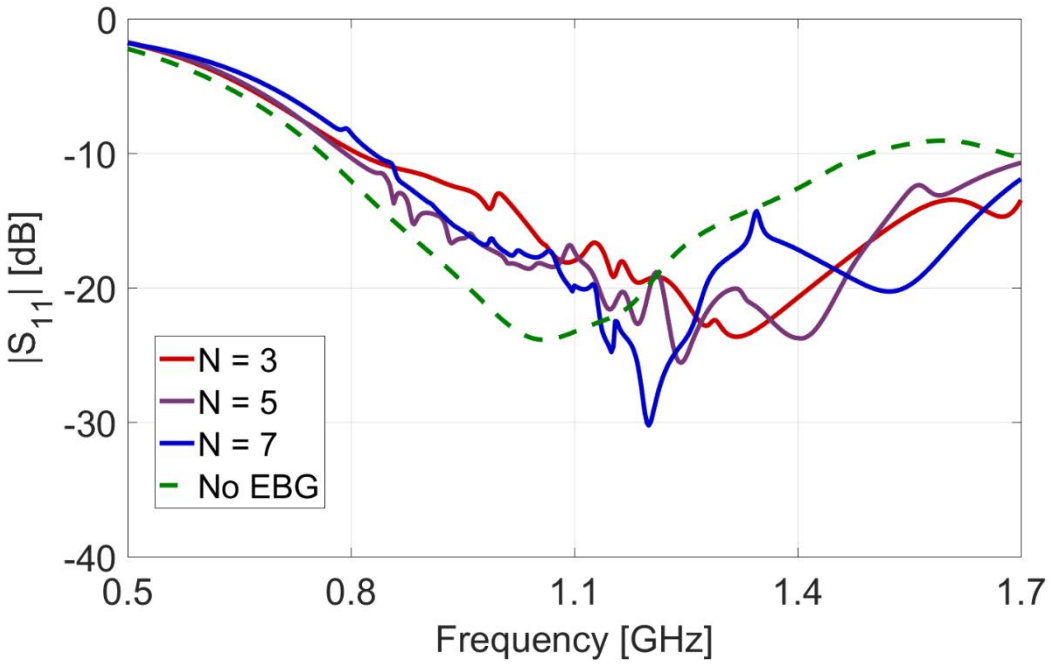

Figure 3.8: S11 for hybrid substrate of Figure 3.6 with EBG dimensions as in Table 2.2.

Because the EBG patches on the hybrid substrate were larger (w = 44 mm) than on the original TMM design, antenna spacing was increased to 600 mm to allow greater N value to be observed. All subsequent monopole simulations will also be performed with a nominal 600 mm antenna spacing. While the previous sweep went up to N = 7, this allowed N to be increased to 11. The S-parameter plots are shown below in Figure 3.10 and Figure 3.11. Change in S11 behavior compared to the last case is negligible. Cases of N = 9 and N = 11 columns both show vastly improved S21 performance over anything seen up to this point. Both have deep valleys close to the center frequency and display greater than 10 dB isolation improvement for bandwidth greater than the cases with fewer EBG columns.

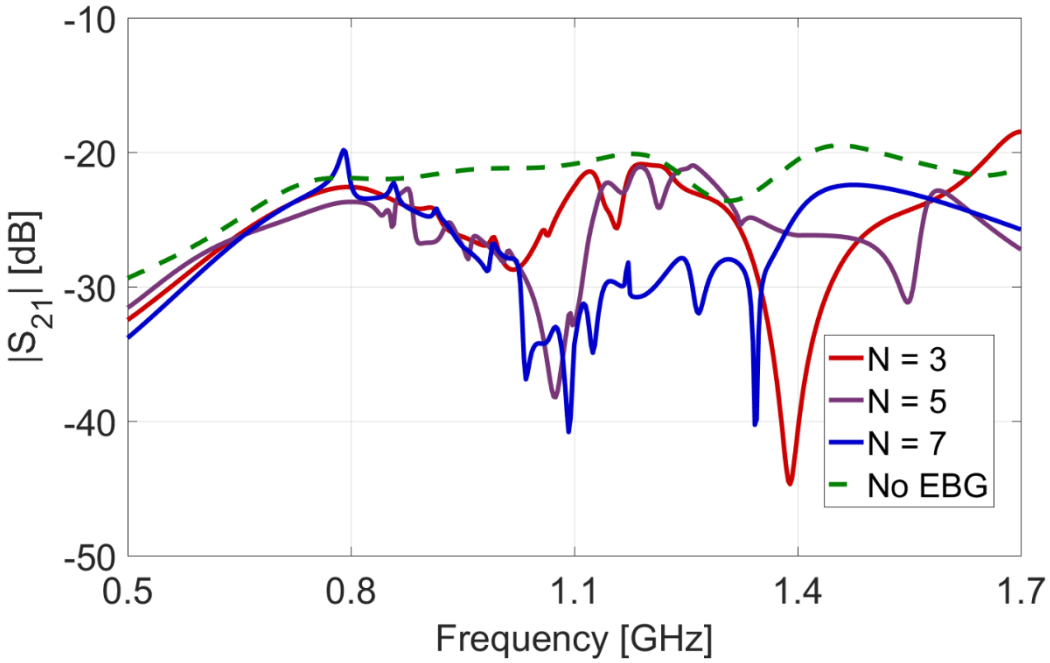

Figure 3.9: S21 for hybrid substrate of Figure 3.6 with EBG dimensions as in Table 2.2.

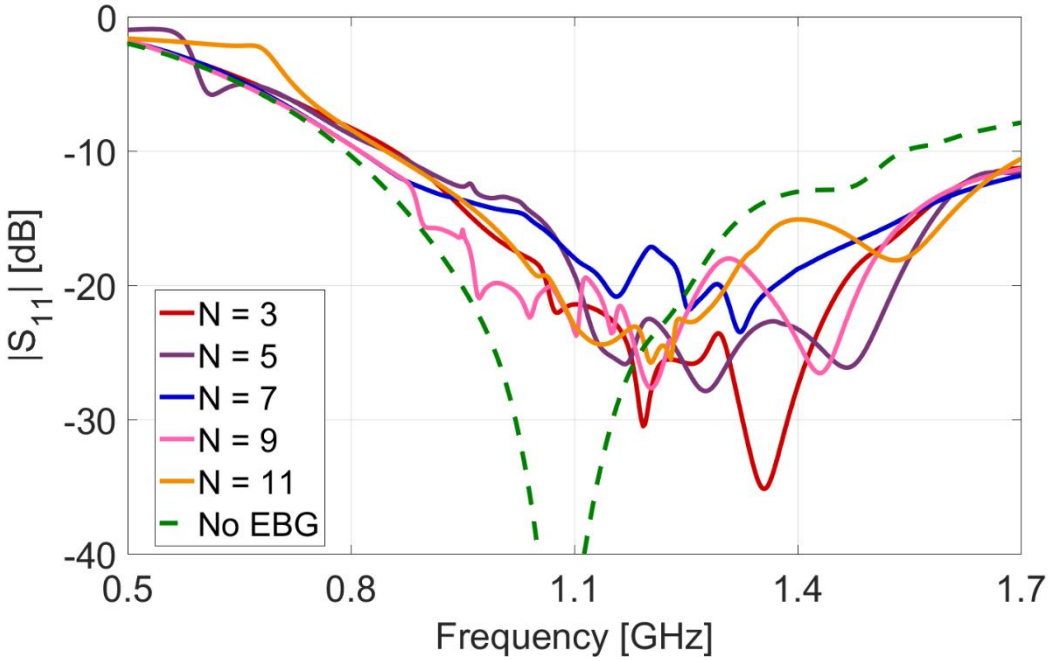

Figure 3.10: Antenna S11 for increased values of *N* on hybrid substrate of Figure 3.6 with EBG dimensions as in Table 2.2.

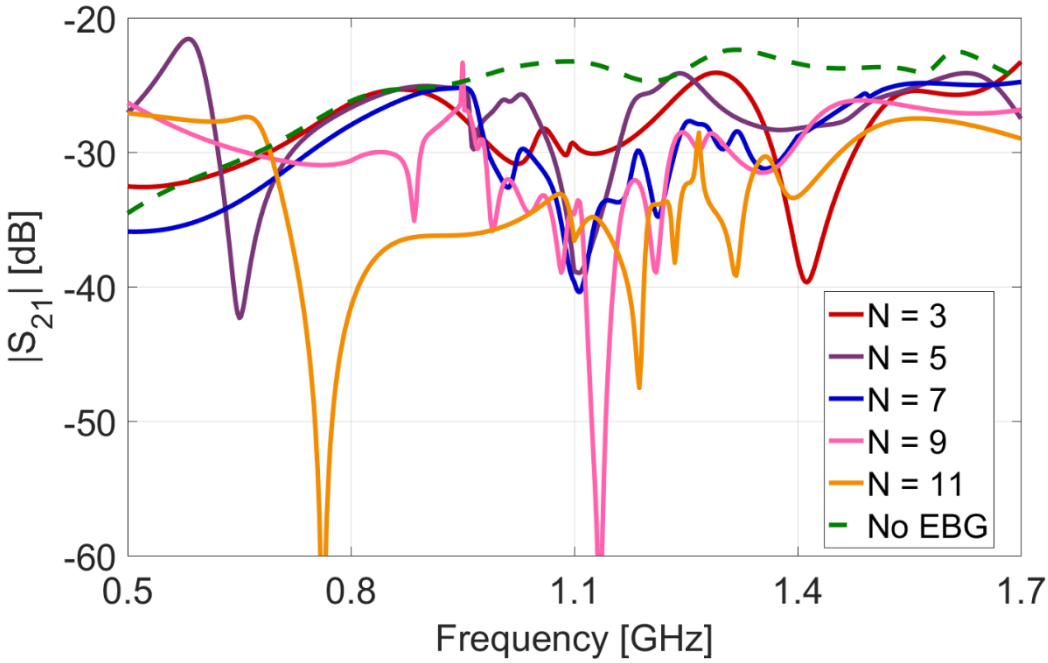

Figure 3.11: S21 for increased values of *N* on hybrid substrate of Figure 3.6 with EBG dimensions as in Table 2.2.

3.5 MULTILAYER EBGS

The previous design with a hybrid substrate became the default case and work was done to observe the effect of stacking these layers on top of each other. In order to do this without shorting the devices, a polyimide layer of 5 mil thickness was used as an insulator between the top ground plane and the bottom patches. This is represented in Figure 3.12 by the green layer. The ground planes were connected by creating a copper wall in the HFSS model on one side of the stack. The individual layer dimensions stayed the same as the previous design, resulting in a total device height of 30 mm + 5 mil (~0.13 mm) of insulation. The number of layers is treated as a new design parameter from here forward and is referred to as *Nz*.

Frequency sweeps were performed as before for cases of 9 and 11 columns. Below in Figure 3.13 and Figure 3.14 are the S-parameter plots for the no-EBG case as well as *Nz*

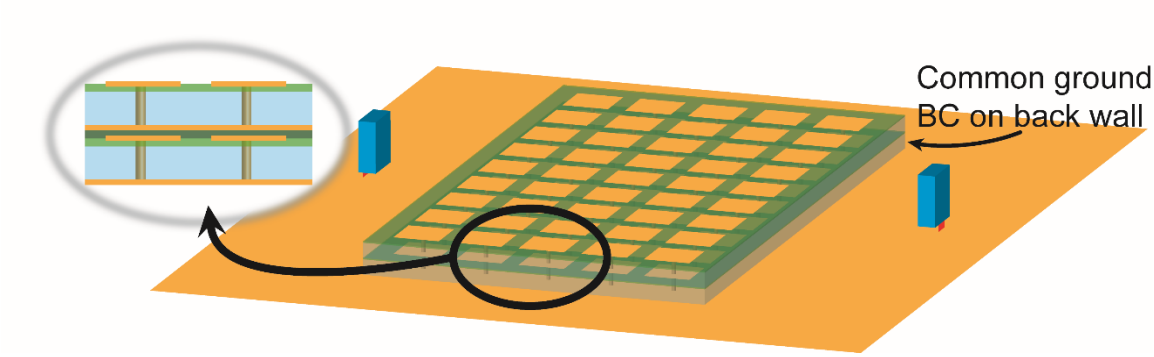

Figure 3.12: Cross section of EBG stackup.

values of 1 and 2 for N = 9. Note that for Nz = 1 total EBG thickness is 15 mm while for Nz = 2 total EBG thickness is 30 mm. The S11 performance, although not as deep as the control case, still maintains sufficient -10 dB bandwidth. The S21, however, shows a remarkable increase in isolation performance. The single layer case had a 20 dB isolation improvement bandwidth of only 2.7%, but the two-layer stackup has over 23% bandwidth in the low end and still shows approximately 15 dB improvement in the higher end of the operating band.

Figure 3.14 shows by far the most interesting results so far. It is clear that the coupling reduction between 750-1000 MHz is between 22-31 dB for Nz = 2. This is a bandwidth of 27.8% whereas the L-band bandwidth requirement is 23.8%. The challenge is to move the band-reject response of 750-1000 MHz found in Figure 3.14 to the frequency band of 960-1220 MHz. A straightforward thought is to just scale the EBG patch width, w and the gap, g. Perhaps the height may also have to be reduced. The moment the patch width and distance are changed the distance from the antenna edge to the nearest patch edge will also change.

Simulations were also conducted for N = 11 and Nz = 2. These results are plotted in Figure 3.15 and Figure 3.16. For N = 11 there was slightly more upshift in S11 than in

the $N = 9$ case. It was later determined that this was due to coupling of the EBG patches to the antennas. The S21 showed a similar level of 20 dB isolation improvement bandwidth increase as for $N = 9$, increasing from 0.8% in the single layer case to 22% for two layers.

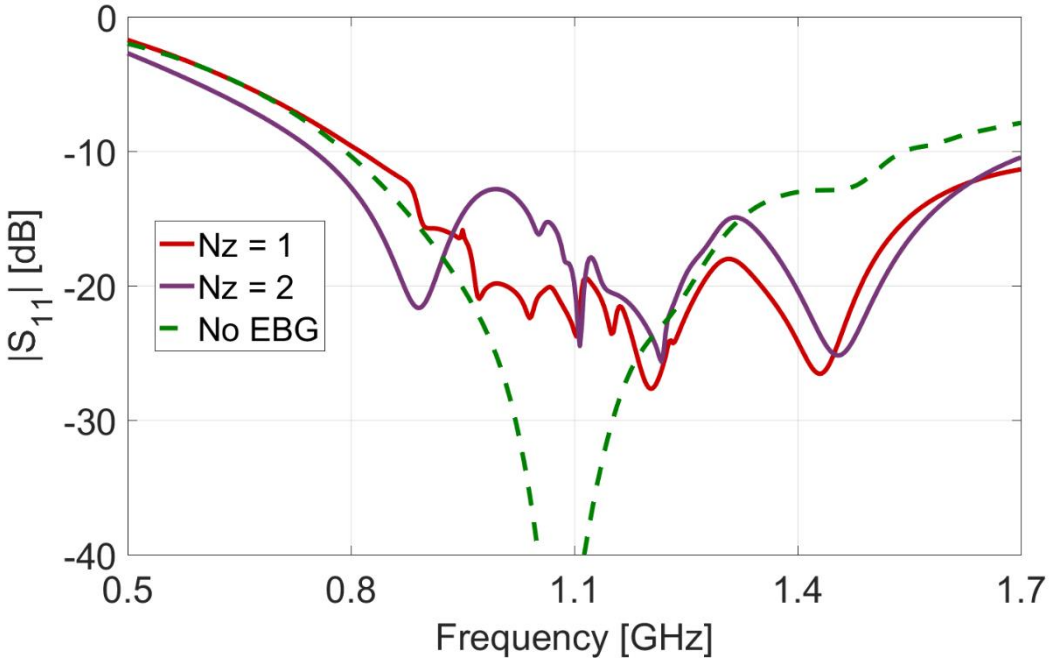

Figure 3.13: S11 for single-layer and two-layer EBG stackups – $N = 9$ and EBG dimensions as in Table 2.2.

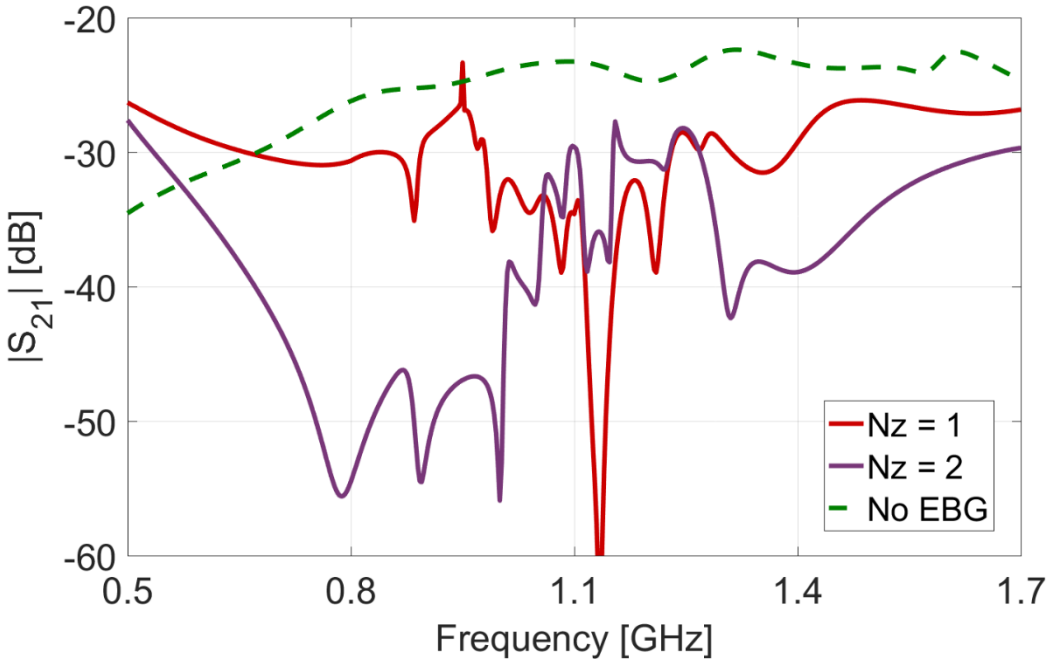

Figure 3.14: S21 for single-layer and two-layer EBG stackups – *N* = 9 and EBG dimensions as in Table 2.2 .

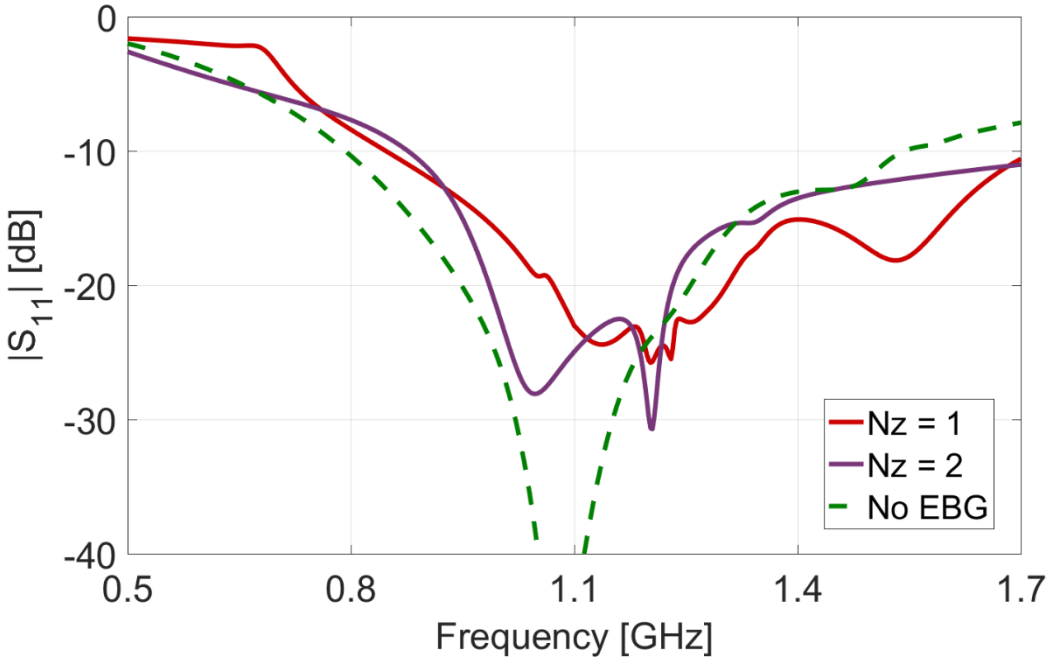

Figure 3.15: S11 for single-layer and two-layer EBG stackups – *N* = 11 and EBG dimensions as in Table 2.2

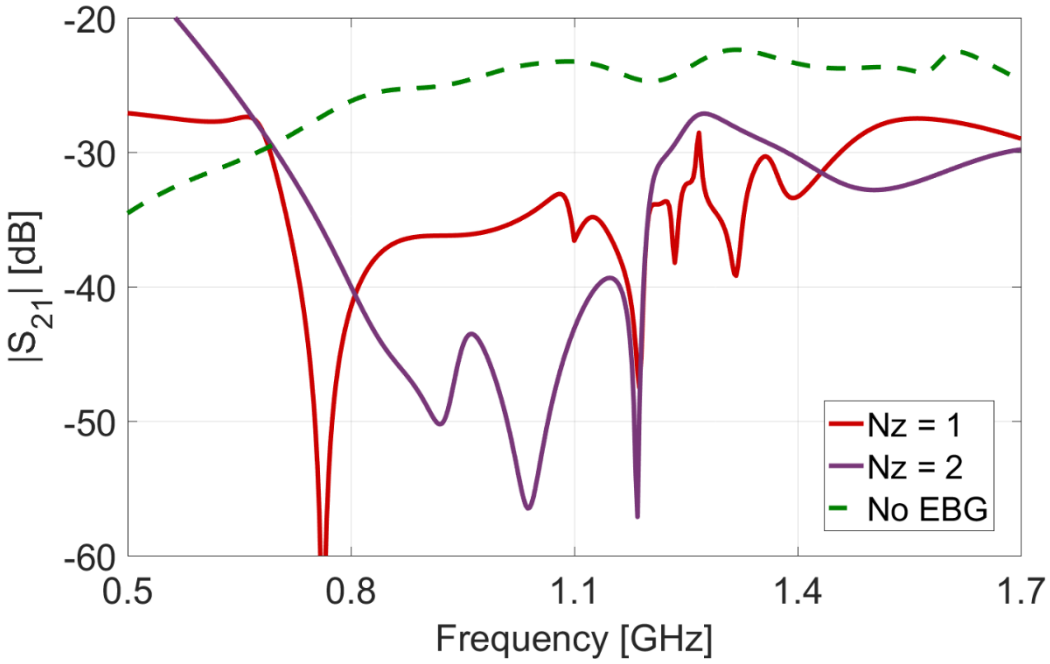

Figure 3.16: S21 for single-layer and two-layer EBG stackups – N = 11 and EBG dimensions as in Table 2.2.

CHAPTER 4: MULTILAYER EBGS WITH PRACTICAL L-BAND BLADE ANTENNAS

At this point in the design process, a more realistic antenna for the EBG application was selected for the simulations. The Sensor Systems antenna S65-5366-10L was selected as a case study and an equivalent antenna was modeled in HFSS, shown in Figure 4.1. The relevant specifications from the datasheet are shown in Table 4.1 below and the VSWR plot for the HFSS model is shown in Figure 4.2. The resulting antenna design was 64 mm tall and 2.54 mm thick.

Table 4.1: Blade antenna VSWR specifications

Operating frequency	960 – 1220 MHz
VSWR	≤ 1.4:1 (1000 – 1100 MHz) ≤ 1.7:1 (960 – 1220 MHz)

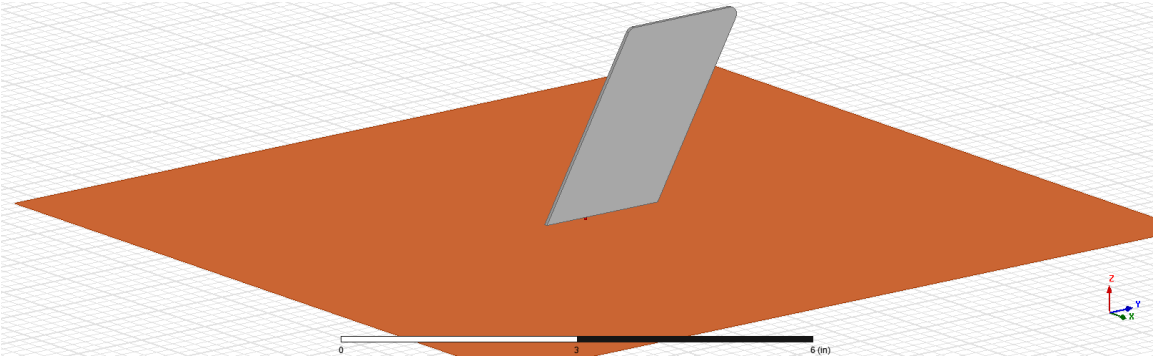

Figure 4.1: Blade antenna 3-D view in HFSS (ground plane size for illustration only).

These antennas were placed broadside to the EBG, meaning the wide edge of the monopole was in parallel to the EBG patch edge. With this more practical antenna in place, a large number of variations were performed to identify any trends or relationships in the

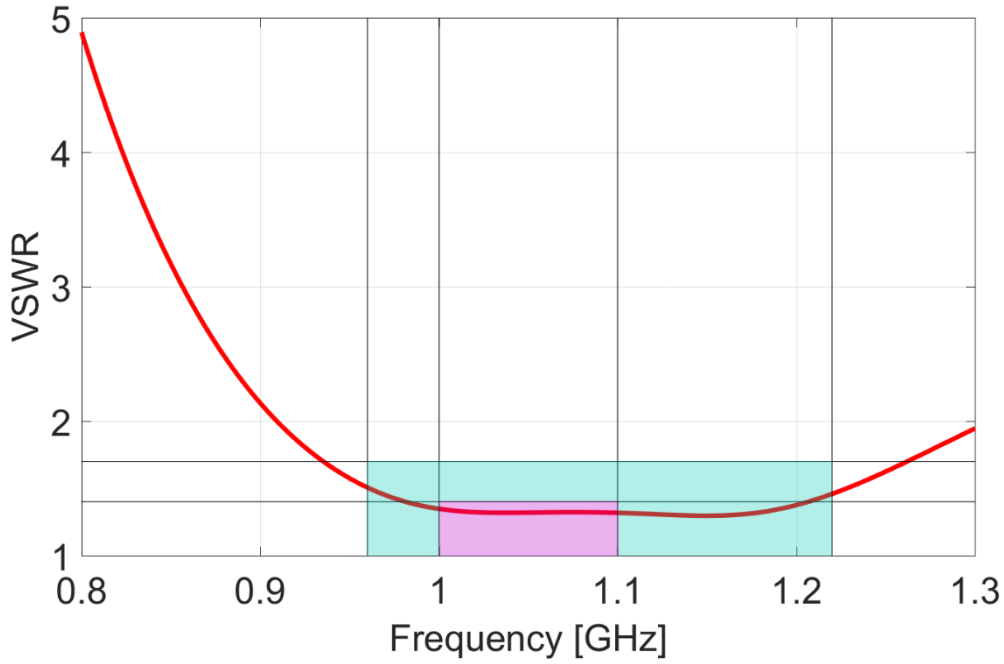

Figure 4.2: VSWR for structure in Figure 4.1 with markers indicating design bounds given in datasheet.

three main design parameters, namely substrate height, patch width, and gap between patches. In this run, 96 variations of dimension combinations were performed. Width varied from 40 to 43 mm, foam height varied from 12.5 to 14 mm (with constant 0.5 mm TMM height), and gap varied from 1 to 2 mm. Among these, having a patch width of 40 mm and foam height of 14 mm yielded the most promising S21 results. The best-case parameters are displayed in Table 4.2 and the S21 plot for these is shown in Figure 4.3.

Table 4.2: EBG dimensions for best-case with *Nz* = 2.

Design Parameter	Size (mm)
Height (total) h	14.5
Width w	40
Gap w	1.2, 1.6, 2.0

Since a 40 mm patch width best-case was at the bounds of the parametric sweep, two more simulations were performed for a patch width of 35 mm and 32 mm. All other dimensions remained the same as before. Shown in Figure 4.4 are the S21 plots for 32, 35,

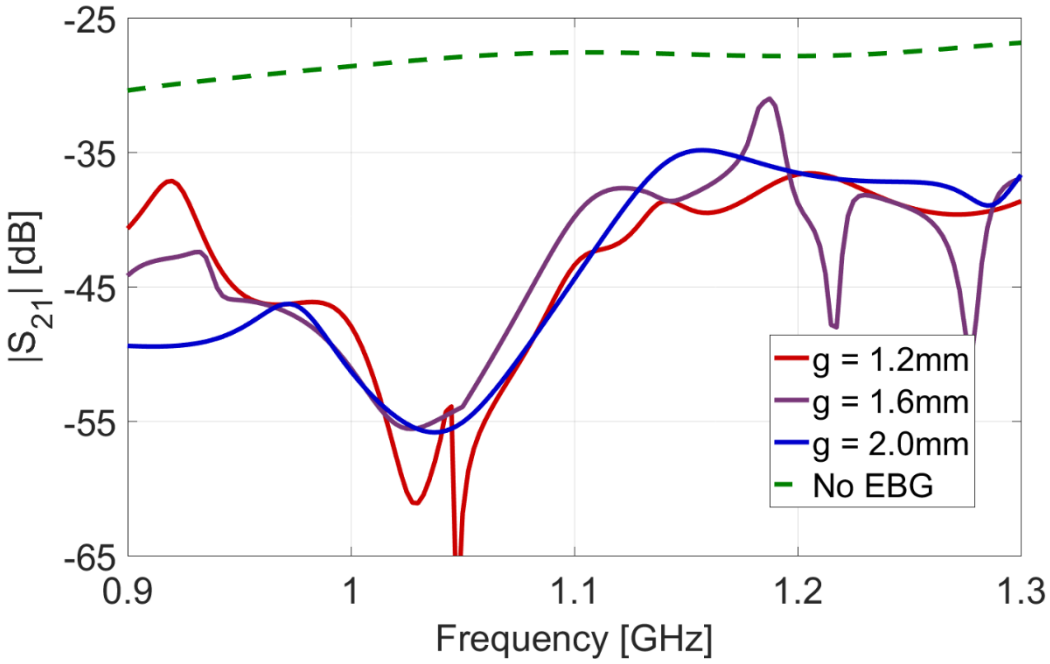

Figure 4.3: Best S21 cases for big sweep with blade antennas – *N* = 9 with EBG dimensions as in Table 2.2.

and 40 mm along with the control case. As indicated by the black dashed line, a patch width of 32 mm provides at least 20 dB of isolation improvement over the control case from approximately 992 to 1300 MHz. Although the starting frequency is slightly higher than 960 MHz, the 301 MHz or 26% bandwidth provided is evidence that sufficient isolation improvement bandwidth can be achieved for an L-band design.

Unfortunately, all of these designs negatively affect the S11 by shifting the low-end -10 dB point up by at least 50 MHz and up to 100 MHz, as shown in Figure 4.5.

Table 4.3: Best case EBG dimensions for *Nz* = 2, *N* = 9.

Parameter	Value (mm)
w	32
g	2
h_{total}	14.5

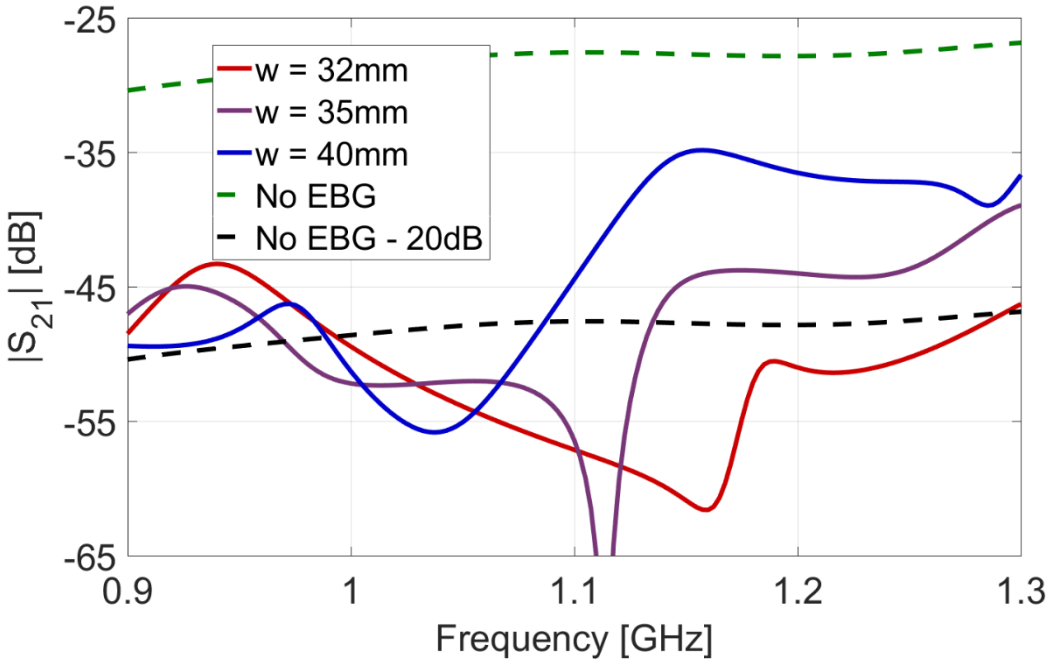

Figure 4.4: S21 for 32, 35, and 40 mm patch width – all other design parameters the same as previous case.

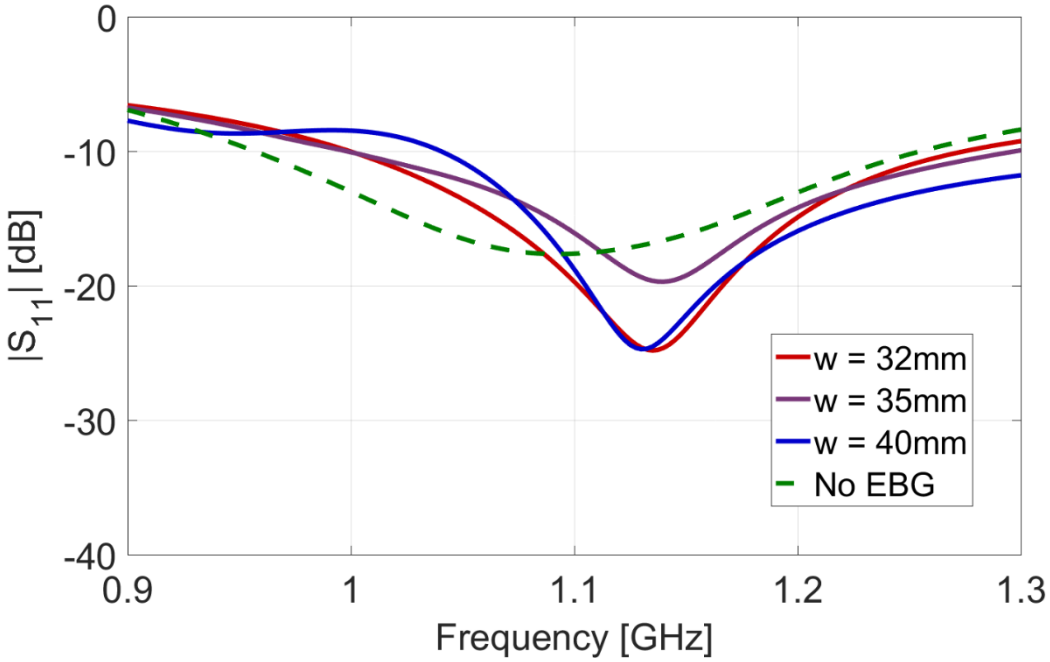

Figure 4.5: S11 for 32, 35, and 40 mm patch width – all other design parameters the same as previous case.

Of these S-parameter curves, the 32 mm shows the best S21 performance by far based of both reduction depth and bandwidth coverage. The dimensions for this best case are shown in Table 4.3.

At this point it was clear that the current EBG design was consistently detuning the antenna's S11 performance by an unacceptable amount. It was theorized that the EBG patches for higher *N* values were encroaching too far into the near field of the antennas and capacitively loading them, resulting in the upshift in S11 observed. The simplest remedy was to increase the distance between the EBG structure and the antennas was to investigate behavior for lower *N* values. The detuning nature shown with the larger EBG structure diminishes as a function of reducing *N*, as indicated by Figure 4.6. Unfortunately the S21 performance is also diminished significantly with decreasing *N* (Figure 4.7), reducing coupling about half as effectively as the larger structure. Of these, $N = 5$, was considered to be the best compromise of performance and size to be further investigated.

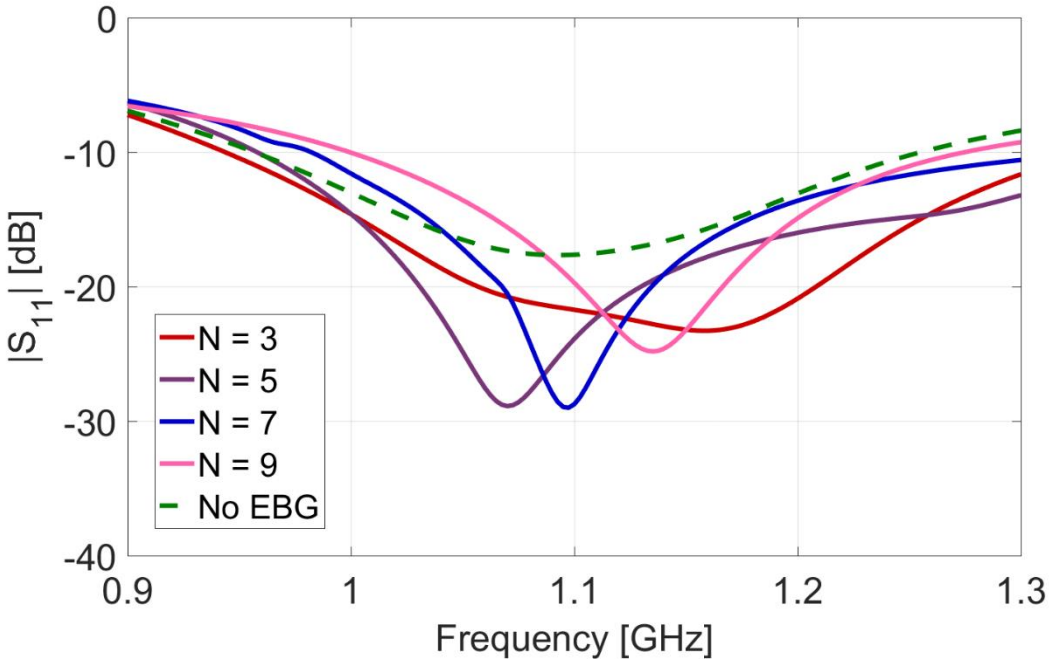

Figure 4.6: S11 behavior for lower *N* values – EBG dimensions as in Table 4.3.

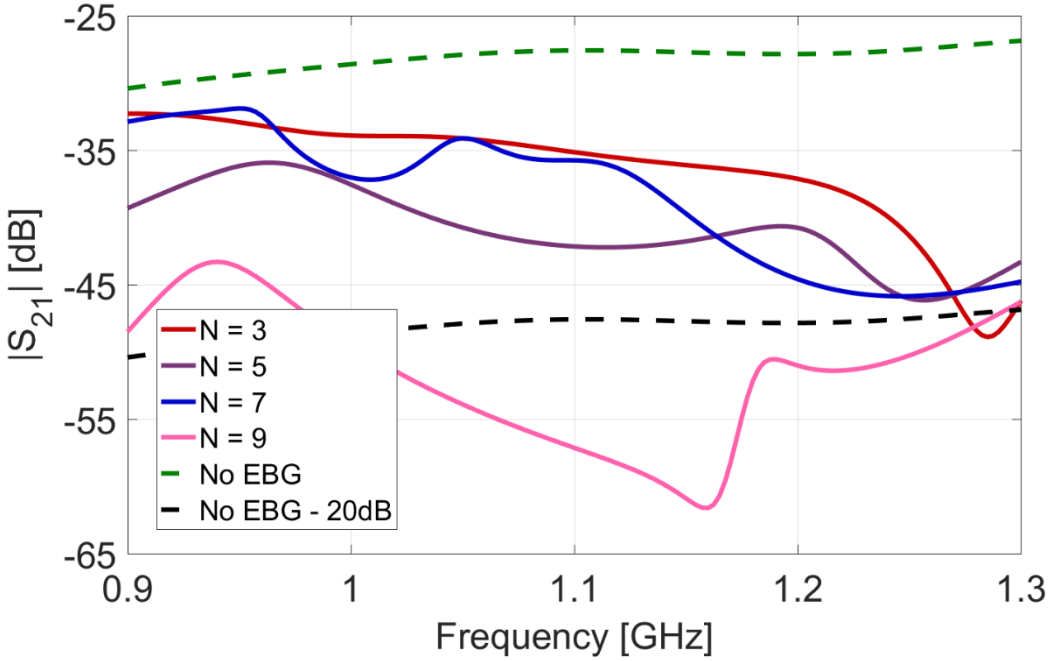

Figure 4.7: S21 behavior for lower *N* values – EBG dimensions as in Table 4.3

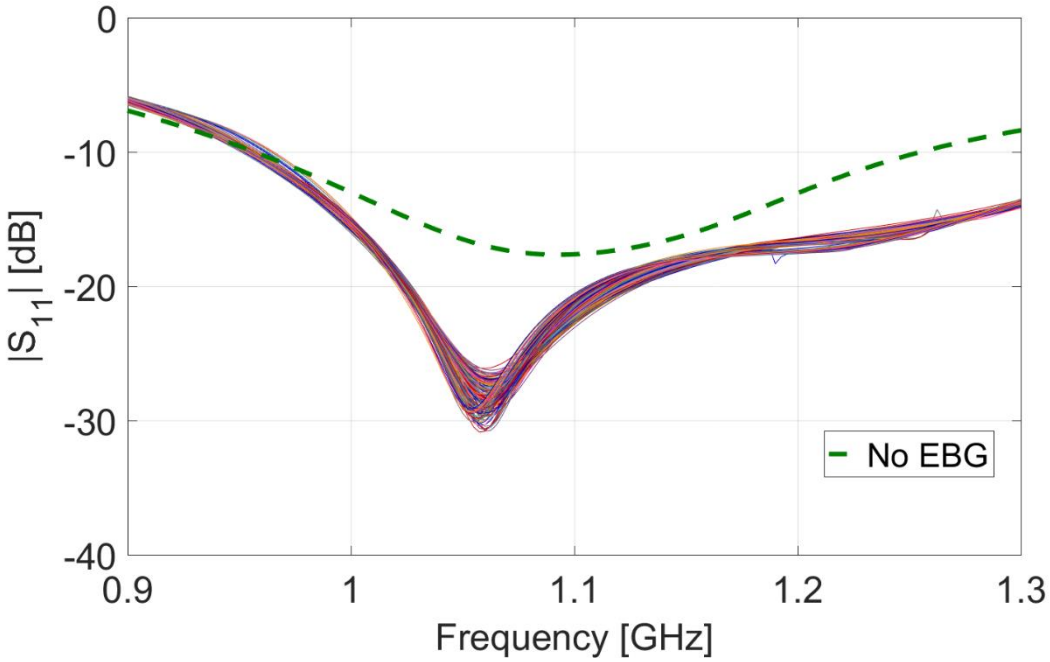

Figure 4.8: S11 results for parametric sweep of EBG dimensions fixing *N* = 5 and *Nz* = 3.

To recover and improve S21 performance, an additional layer of EBG was added on top in the same way the second layer was added to the first. It was theorized at first that the total height should remain constant between $Nz = 2$ and $Nz = 3$, resulting in thinner individual layers for the new structure. The results of this showed no indication of L-band tuning in any configuration tested and the original layer thicknesses were restored to all three layers. A parametric sweep of *w*, *g*, and *h* was once again performed with three layers. Width varied from 28 to 33 mm, foam height varied from 12 to 14.5 mm (with constant 0.5 mm TMM height), and gap varied from 1.6 to 2 mm. The results of these variations are shown in Figure 4.8 and Figure 4.9. In reducing *N* from 9 to 5, the distance between the outermost EBG patch edges and the closest points on the respective antennas was increased from approximately 147 mm to approximately 220 mm, with slight variations due to patch width and gap size. This significantly improved the S11 tuning (Figure 4.8), with all variations having a low-end -10 dB point within an approximately 15 MHz range, with no single variation being detuned greater than 9 MHz off of the nominal case. The S11 results clearly illustrate the need for enough separation between the EBG edge and the antenna to avoid antenna detuning.

The family of coupling curves (S21) shown in Figure 4.9 illustrate the sensitivity of the responses due to *w*, *g*, and *h* variations, with some having more influence than the others. Multiple resonances are observed along with signs of wide responses with wide band coupling reduction potentials. Many of these traces were selected, highlighted, and examined one after another to identify the ones that have the best potentials for coupling reductions. In order to elucidate the effects of these variations several plots were generated with fewer parameters variations.

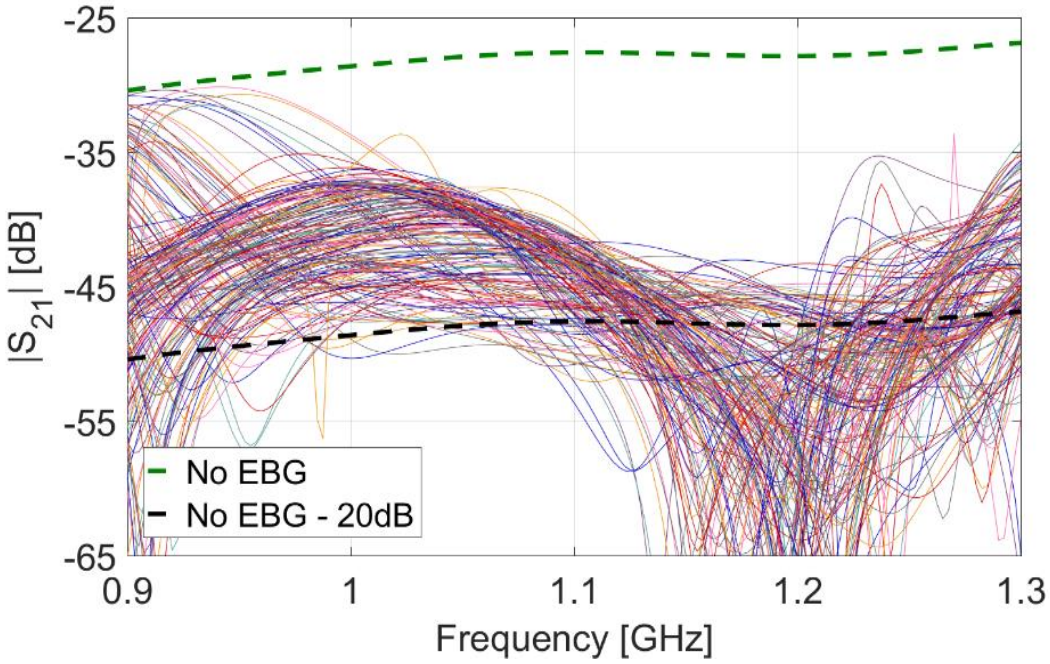

Figure 4.9: S21 results for parametric sweep of EBG dimensions fixing N = 5 and Nz = 3.

Figure 4.10 shows the effects of varying the parameter *g*. It is clear that as *g* varies from 1.6 to 2 mm the overall S21 response is not affected in any significant manner. Interestingly, with these parameters about 40 dB coupling reduction around 1.2 GHz is possible. The lowest amount of coupling reduction is about 12 dB within the 960-1220 MHz band.

Figure 4.11 shows the effects of varying the parameter *w*. It is clear that as *w* varies from 28 to 33 mm the overall S21 response is significantly affected. It is clear that in all cases the response shows a dual or multiple resonance phenomenon that exhibits low S21 magnitudes. For *w* = 32 and 33 mm the resonance at the low end of the band occurs below 900 MHz and is thus of no value for our particular L-band blade monopole. As *w* is decreased further the two resonances start to come closer. This is especially true for the case where *w* = 28 mm, in which one resonance can be seen around 940 and another at around 1.24 GHz. These two together offer a wide S21 response allowing coupling

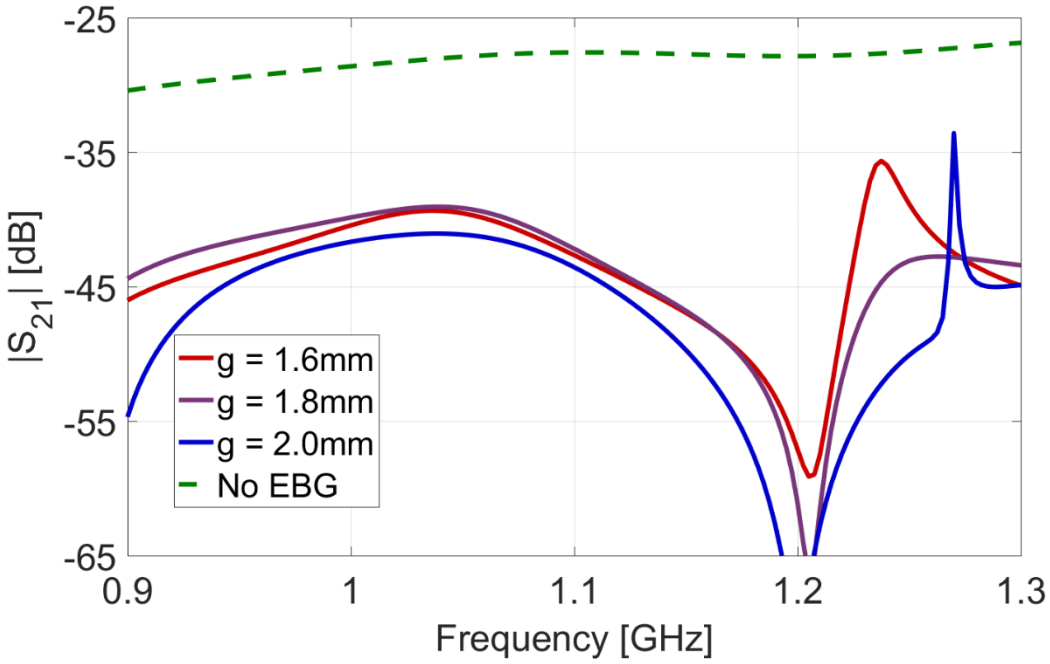

Figure 4.10: S21 results for *g* variation only, fixing *w* = 30 mm, *h* = 14.5 mm.

reduction between 18 to 23 dB. This behavior clearly resembles that of a stacked microstrip patch antenna [28] where a smaller patch couples to a larger patch and allow a wide band response. In general, the dimensions of the two patch antennas and their substrate heights must be optimized to obtain a wideband response. Alternatively, a dual-band response can be obtained where the two resonances are separated by a much larger frequency range with a mismatch in the middle of the band. The EBG plus L-band antenna scenario is analogous to the stacked patch antenna in a sense that the EBG structure contains three layers and it is the inter-layer coupling that either allows a multiband response with deep S21 poles or a wideband response with a nearly constant S21 response. It is clear that for narrowband cases, even multi-band systems, much larger coupling reduction is feasible at discrete bands. For wideband cases some form of optimization would be recommended to obtain the desired response.

These observations prove to be correct when the third EBG parameter, *h* is varied as shown in Figure 4.12. Similarly to the variation of *w*, the variation of *h* also allows significant control of the S21. Note that for *h* = 12.5 mm greater than 20 dB coupling reduction is obtained from 980 MHz to 1240 MHz. Coupling reduction at 960 MHz, the lowest edge of the target band, is still 15 dB.

Several cases are compared in Figure 4.13 that summarize some of the notable results. Note that for *Nz* = 2, *N* = 9 although the amount of coupling reduction throughout the entire band is better than the others it detunes the antenna by about 20 MHz to a higher frequency. The other two cases exhibit similar performance to the best case from the previous design of *Nz* = 2, *N* = 9. Both of these new designs have a patch width of 30 mm, as opposed to the 32 mm seen before, and differ slightly in height and gap. The design with a foam spacer height of 12.5 mm and a gap of 2 mm shows a 20 dB improvement bandwidth from 980 MHz to 1240 MHz, or approximately 23.4%. The coupling reduction at the lower design bound of 960 MHz is -15.1 dB. More importantly, the lower -10 dB S11 crossover point is completely preserved when the EBG is installed. This is shown in Figure 4.14. Simulated patterns for this case are shown in Figure 4.15 where the green traces represent the patterns for the no EBG case and the red traces represent the patterns for the final optimized EBG case. As seen, the elevation plane patterns for the two cases are nearly identical in the $\varphi = 0^o$ plane. There is some asymmetry observed in the $\varphi = 90^o$ plane or the EBG plane due to the presence of the EBG. Observing the azimuthal pattern ($\theta = 90^o$) the EBG causes only minor non-uniformity in the pattern.

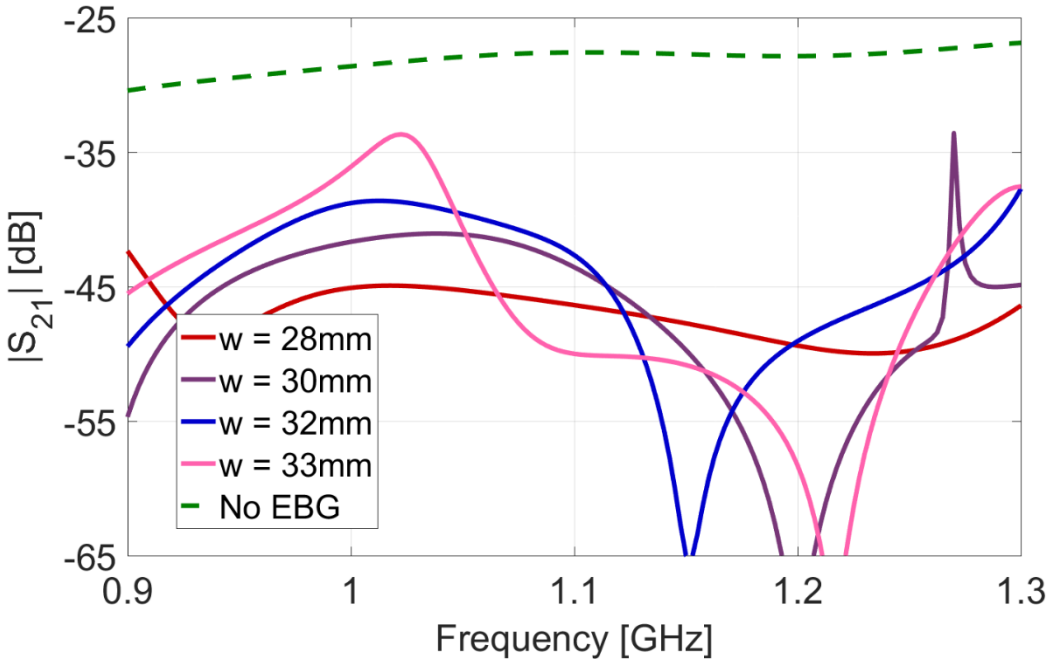

Figure 4.11: S21 results for *w* variation only, fixing *g* = 2 mm, *h* = 14.5 mm.

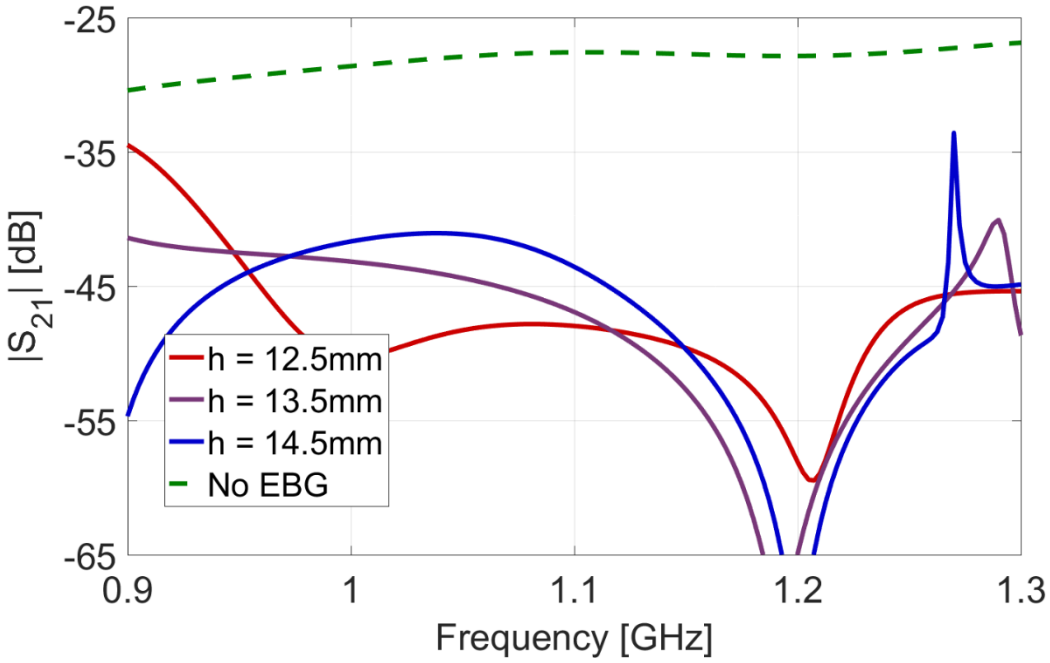

Figure 4.12: S21 results for *h* variation only, fixing *w* = 30 mm, *g* = 2 mm.

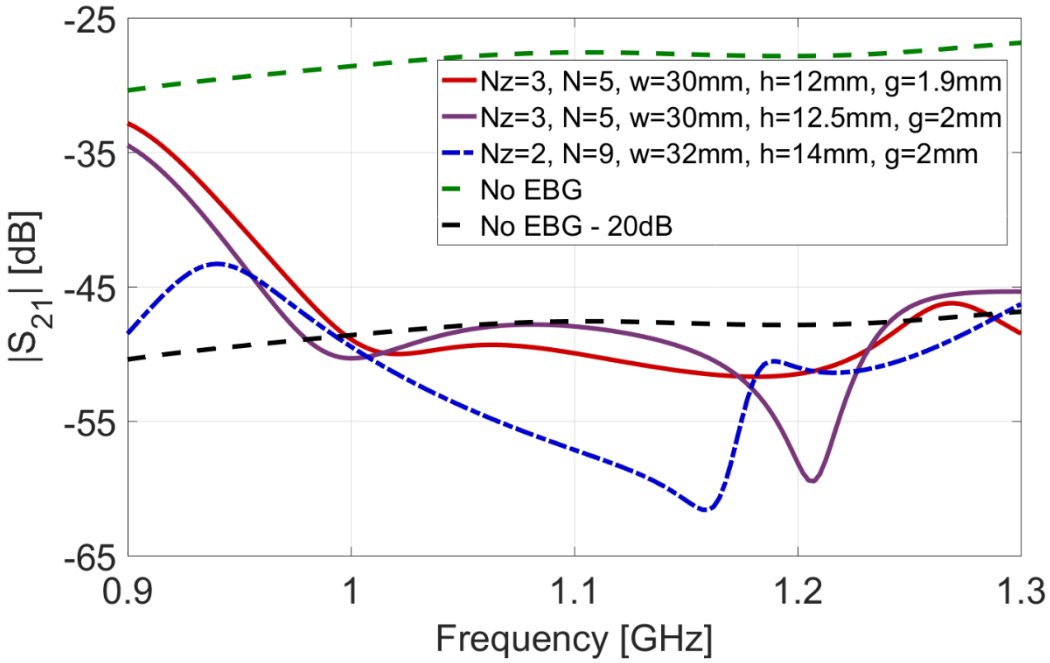

Figure 4.13: Comparison of best-case S21 results for previous *Nz* = 2, *N* = 5 structure and more compact *Nz* = 3, *N* = 5 structure

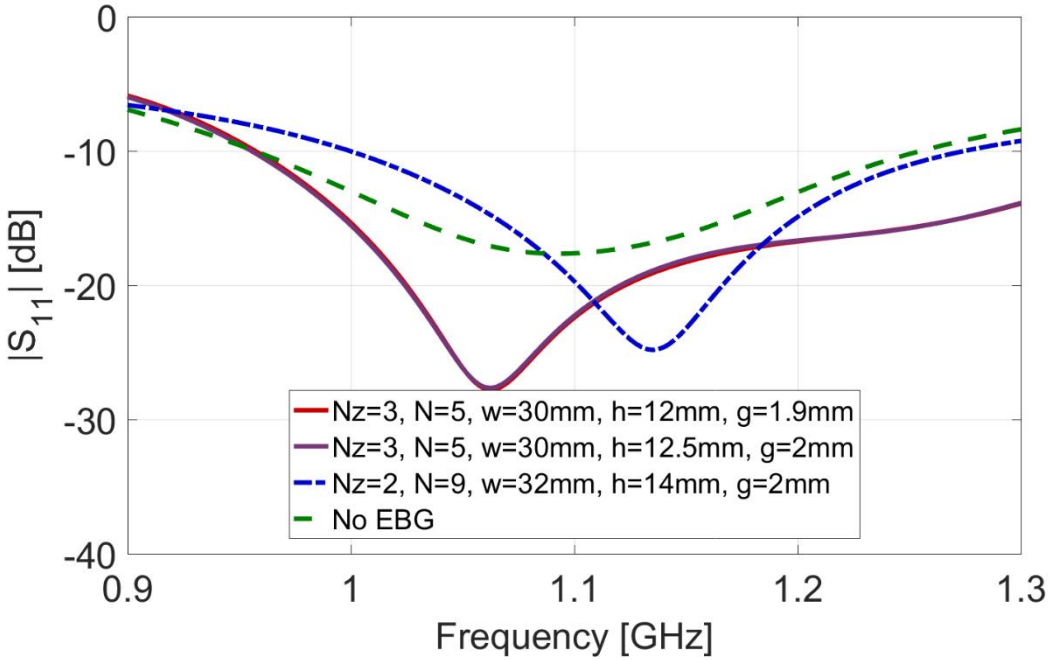

Figure 4.14: Comparison of best-case S11 results for previous *Nz* = 2, *N* = 5 structure and more compact *Nz* = 3, *N* = 5 structure.

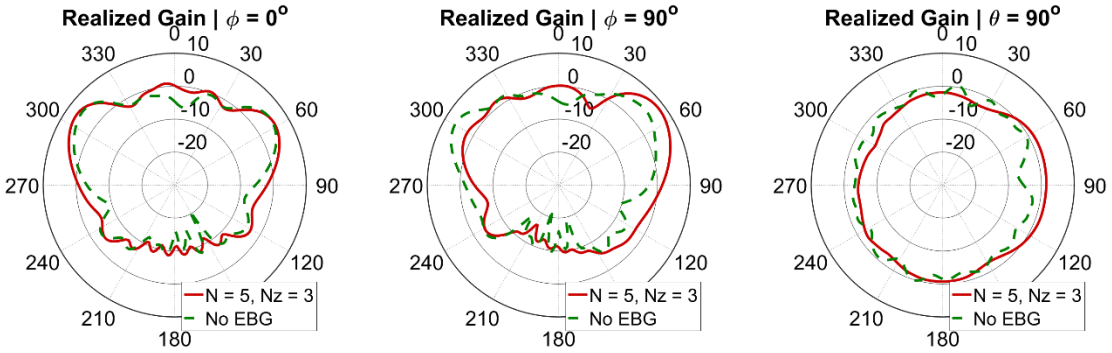

Figure 4.15: Radiation patterns at 1100 MHz for *N* = 5, *N*z = 3

CHAPTER 5: MULTILAYER EBG WITH WIDEBAND PATCH ANTENNAS

As outlined in the introduction section, coupling reduction between two adjacent microstrip patch antennas on the same substrate using EBG structures is well known [19]. Coupling reduction of 10 dB or so is easily achieved over a narrow frequency band using such schemes. Since the multilayer EBG concept developed so far provides far greater coupling reduction and over a broad or multi-frequency band it was investigated further with relation to patch antennas. Wideband aperture coupled patch antennas were designed based on our previous works [25, 26] that can operate in both the L1 and L2 bands. Circular polarization was not considered because it would have required the necessary feed design containing quadrature hybrids [27], but such concepts already exist and are well known. As with the L-band monopoles, a three-layer mushroom EBG structure using hybrid TMM and foam were considered for antenna-to-antenna coupling reduction. Initially, edge-to-edge antenna spacing of 268 mm was considered. The antenna plus EBG arrangements can be seen in Figure 5.1. The EBG parameters were: w = 30 mm, g = 2 mm, and a total h of 13 mm, being divided as 0.5 mm of TMM and 12.5 mm of foam. Nz = 3 for all cases. Simulated S11 data shown in Figure 5.2 demonstrates antenna operation in the L2 GPS band (1220 MHz) for N up to 3. When N is increased to 5 the return loss deteriorates. S21 results in Figure 5.3 show modest coupling reduction between the two antennas in the same frequency band, about 10.5 dB at 1220 MHz for N = 3.

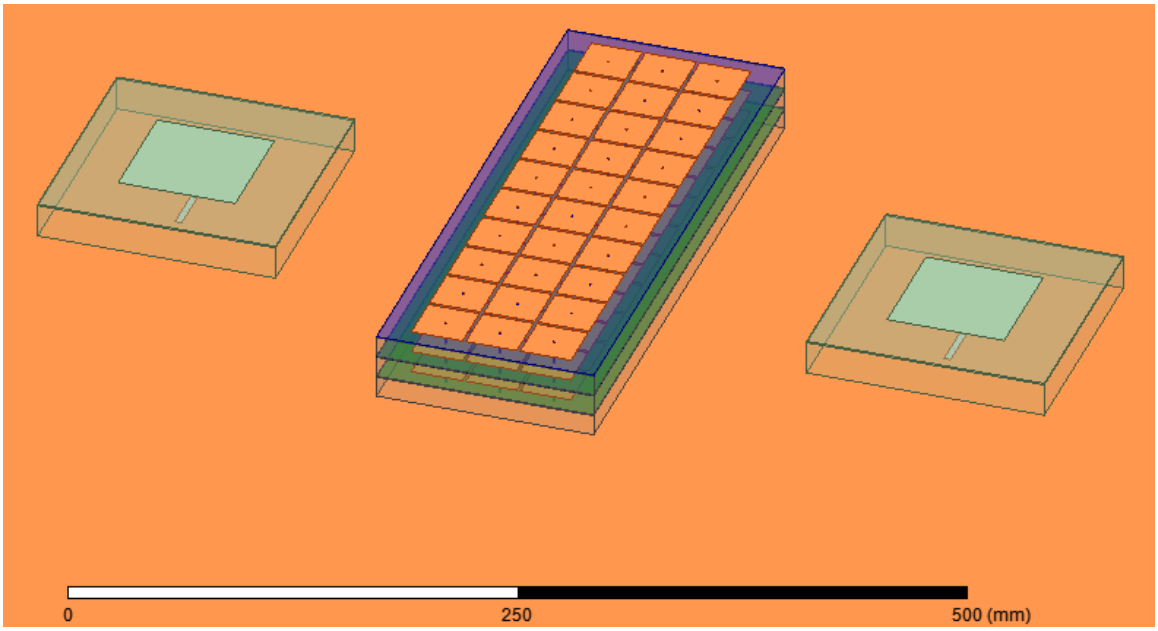

Figure 5.1: Aperture coupled patches with EBGs as seen in HFSS.

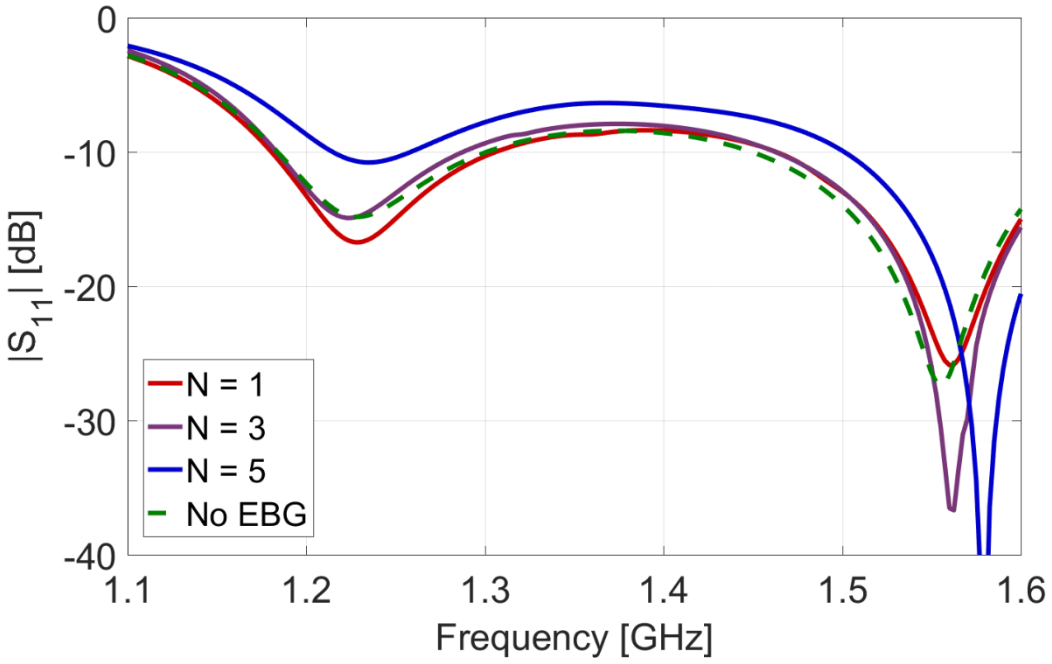

Figure 5.2: Simulated S11 as function of number of EBG columns in between two aperture coupled patches (antenna edge-to-edge distance=268 mm).

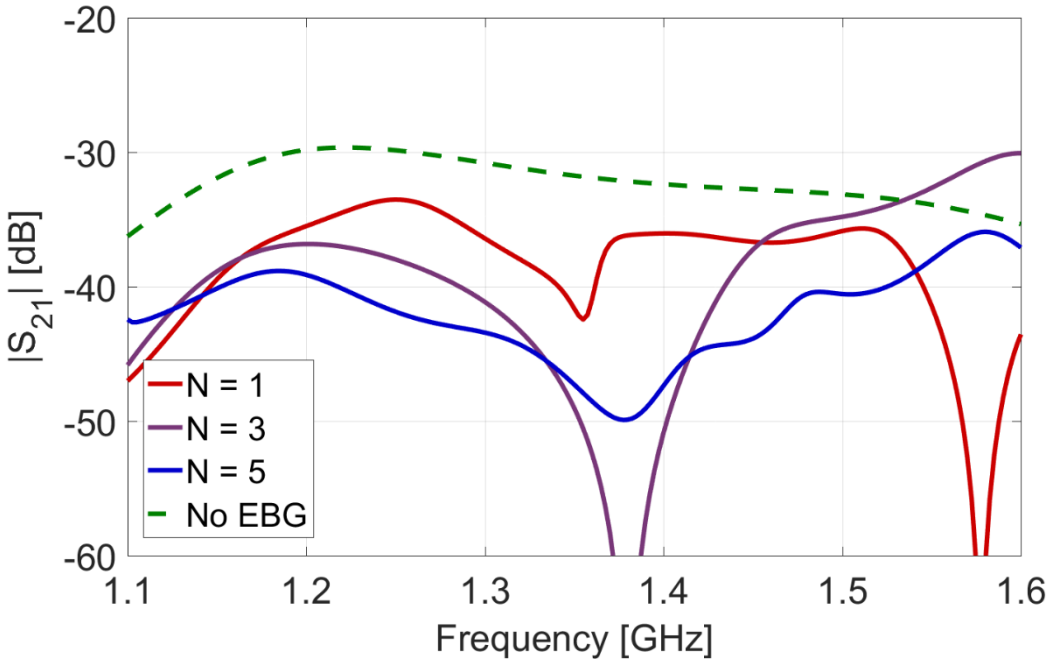

Figure 5.3: Simulated S21 as function of number of EBG columns in between two aperture coupled patches (antenna edge-to-edge distance=268 mm).

Subsequently, the distance between the two patches was increased so that the return loss performance is not affected. Parametric simulations were conducted by varying *w* from 30 to 40 mm in 1 mm increments and *g* from 1.6 to 2.6 mm in 0.1 mm increments. S11 results from these simulations can be seen in Figure 5.4. It is clear that the aperture coupled patch can operate in both the L1 and the L2 bands.

Simulated S21 results plotted in Figure 5.5 show many possibilities for adoption. Note that the green dotted line indicates the coupling between the patches without any EBG while the gray dotted line below indicates the 20 dB coupling reduction from the green dotted baseline. One possibility is highlighted that shows that tremendous amount of coupling reduction can be achieved in the L1 band. Coupling reduction in excess of 30 dB can be achieved at 1575 MHz. The same EBG if adopted would provide almost 20 dB coupling reduction at 1220 MHz. The parameters for this EBG are: w = 31 mm, g = 2.6

mm, and N = 3. The other parameters are constant throughout all variations, namely Nz = 3, h_{foam} = 12.5 mm and h_{TMM} = 0.5 mm.

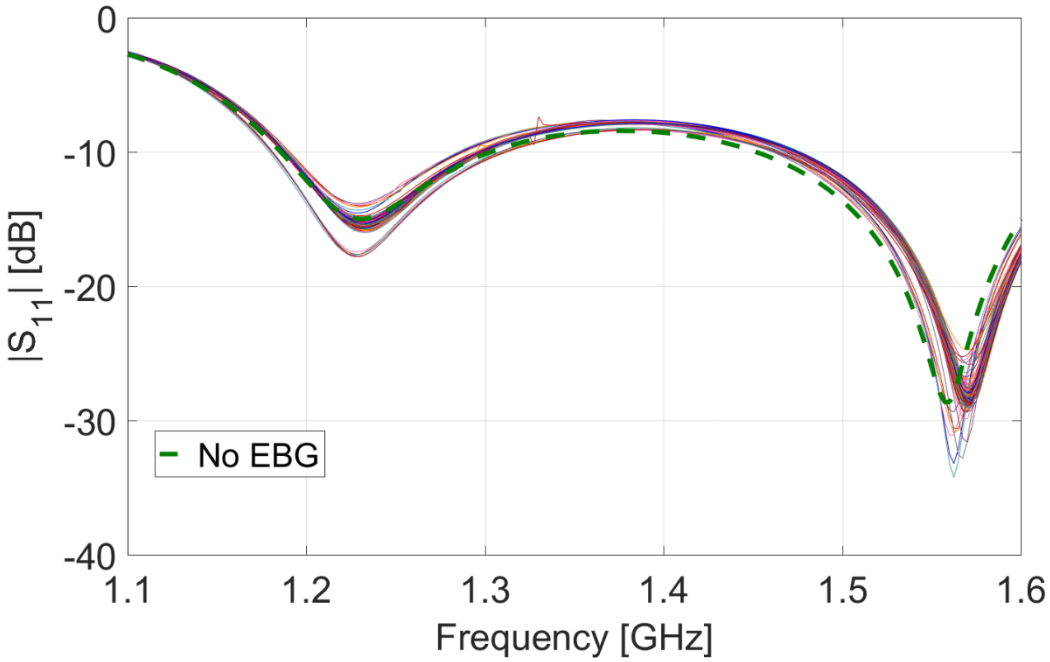

Figure 5.4: Simulated S11 as function of EBG parameters by varying w from 30 to 40 mm at 1 mm increments and g from 1.6 to 2.6 mm at 0.1 mm increments (antenna edge-to-edge distance=384 mm).

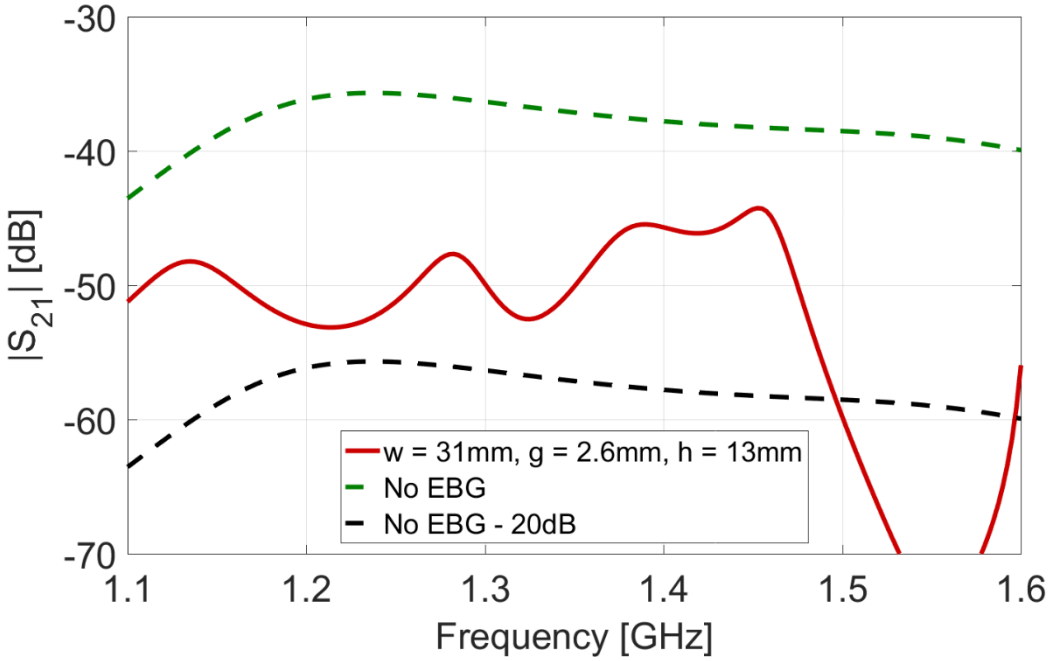

Figure 5.5: Greater than 30 dB coupling reduction shown for L2 in best case.

CHAPTER 6: ANALYTICAL MODEL AND FUTURE WORK

6.1 ANALYTICAL MODEL AND MATLAB MODEL

In order to gain a better understanding of the behavior of the EBG as a coupling reduction tool and how interaction between the design parameters affected the overall performance, work is ongoing to develop a numerical model to describe the structure in terms of its design parameters and predict its performance. The intent of this model is to observe performance trends and assist future design that may allow for a reduction in simulation time.

To begin with this type of analysis, the structure was stripped back down to the most basic form: a single layer EBG on a homogeneous dielectric substrate. Thus a single row of patches were placed on a grounded dielectric substrate. A via was placed at the center of each patch. As a starting point ten patches and vias were considered. The parameters of this simple EBG are listed in Table 6.1.

Table 6.1: EBG parameters for first-order Matlab simulation

Parameter	Value
ε_r	2.2 (PTFE)
W	30 mm
g	2 mm
h	13 mm

Equations (1)-(2) describe the inductance and capacitance that can result from such EBG vias and patches. An equivalent circuit model containing these inductors and capacitors can be seen in Figure 6.1. The capacitive element is a result of adjacent patch

edges and is largely dependent on ε_r, w and g. The inductive behavior is due to the via and is largely a function of h.

Figure 6.1: High-level schematic of first order lumped circuit model of EBG structure.

Considering the circuit model of Figure 6.1, its combined ABCD parameters were calculated using Matlab. The circuit shown in Figure 6.1 was considered to be a standard 2-port network referenced to 50Ω. The combined ABCD matrix was finally converted to S-parameters. Computed S21 data for this model are shown in Figure 6.2, which show a certain degree of bandstop behavior in the simulated band; approximately -7.5 dB at 850 MHz, -6 dB at 1000 MHz, and -5 dB at 1220 MHz. However, given that this model did not contain any information on the source that illuminates the EBG structure e.g. plane wave, monopole antenna etc. further improvements are warranted.

The figure below shows a certain degree of bandstop behavior in the simulated band; approximately -7.5 dB at 850 MHz, -6 dB at 1000 MHz, and -5 dB at 1220 MHz. With this indication of activity in the desired band, work was done to refine the numerical model to more accurately reflect the HFSS design.

From previous HFSS simulations of EBGs near monopole antennas it was observed that the electric field magnitude on the EBG patches varied along the length of each row.

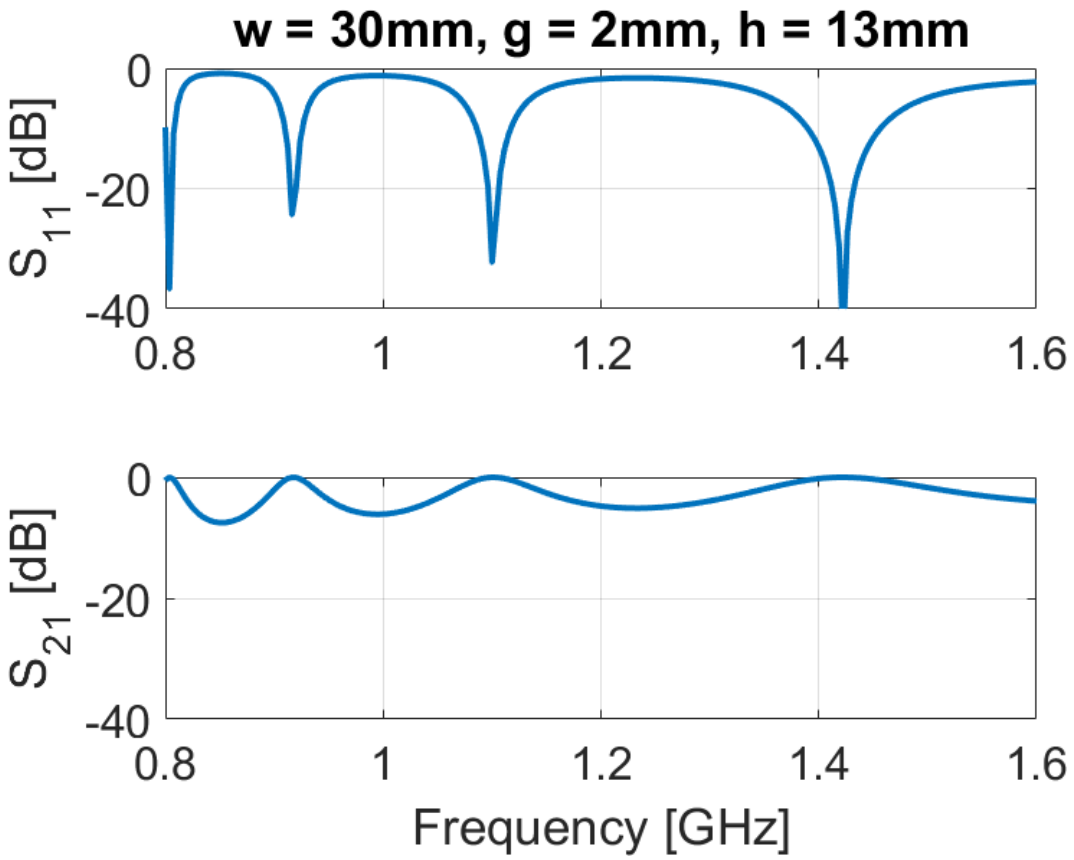

Figure 6.2: S-parameter plots for initial EBG analysis in Matlab.

Note that the simple circuit model shown in Figure 6.1 shows capacitance between the patch edges. All nine capacitance values for the ten-element EBG were the same in the model as were the ten inductance values. Since capacitance is in general inversely proportional to the voltage across a gap, this would mean the gap capacitances are also inversely proportional to the electric field intensity in that region. As such, the first refinement to the analytical model was to include weighted capacitances for each gap dependent on the electric field at those patch edges. To do so, the magnitude of the electric field intensity on each patch edge was computed using HFSS.

This was done as follows: The ten element EBG structure was placed between the blade antennas described before. The resulting electric field plot is shown in Figure 6.3.

The separation between the blade antennas was kept at 600 mm; thus, the distance between the antenna and the nearest EBG patch edge was 141 mm or 0.45λ.

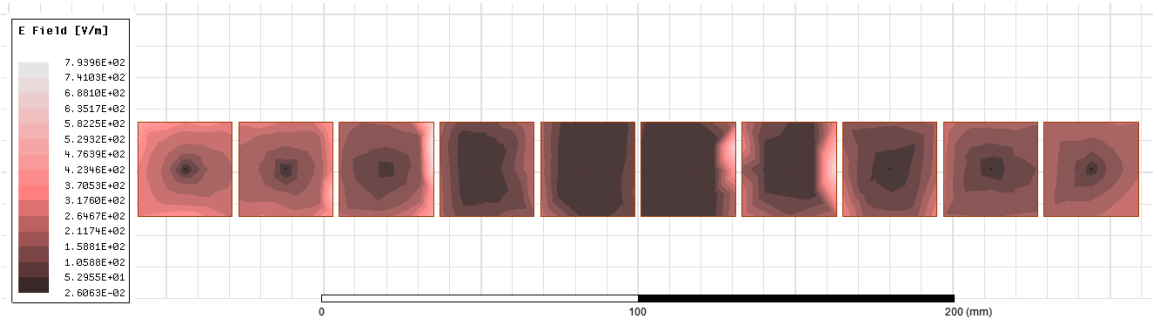

Figure 6.3: Electric field magnitude on EBG patches of the dimensions in Table 6.1.

To derive weighting coefficients for capacitance, the HFSS fields calculator was used to measure the electric field magnitude along adjacent edges. To do so, non-model polyline elements were placed along each edge of the EBG patches where data was to be collected. The green bars in Figure 6.4 highlight the positions of the calculator probes. These lines were used as the geometry along which the fields calculator would collect the precise electric field magnitude data points. The arithmetic mean of the magnitudes along each edge was stored in a data table. Then, the mean magnitudes for adjacent edges were averaged to obtain a single weighting coefficient for each gap capacitance.

Similarly, weighting coefficients were derived for the via inductances by observing the surface currents along the via. To do so, polyline elements were placed along the vertical vias, one line per via, as illustrated in Figure 6.5. This geometry was used to calculate the surface currents along each via. Similarly to the patch calculations, the collected data was arithmetically averaged along the length of the via to obtain a single coefficient for each via's position to be used for weighting inductances.

Figure 6.4: Illustration of E-field probes along patch edges (top view).

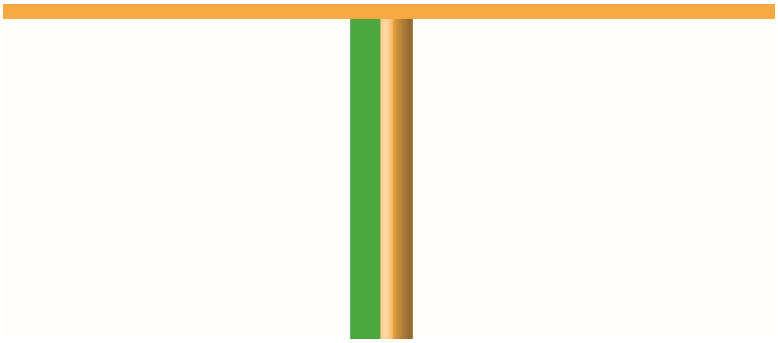

Figure 6.5: Illustration of surface current probe along via length (side view).

Figure 6.6 and Figure 6.7 show the normalized gap capacitance coefficients and via inductance coefficients, respectively. Each set of data was linearly normalized to the set's maximum value so that the maximum coefficient of the resulting set was 1 and all other values landed between 0 and 1.

These values were then loaded as arrays into the Matlab workspace. The functions to compute Z_C and Z_L were modified to distribute these coefficients along each unit cell by direct element-wise multiplication and the resulting matrices were processed into ABCD

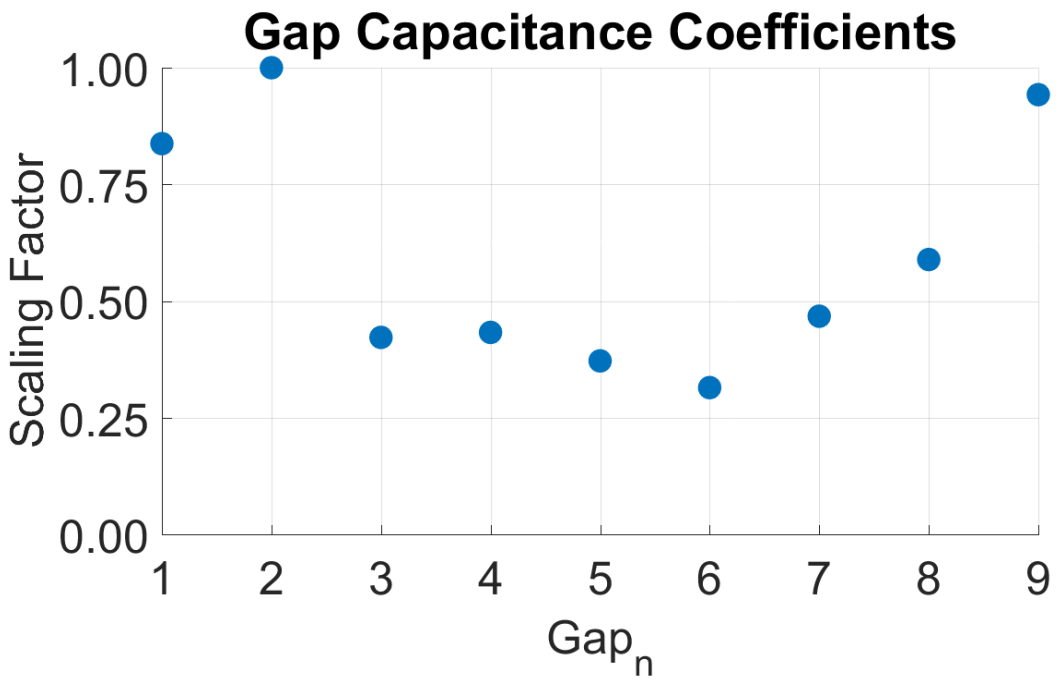

Figure 6.6: Normalized gap capacitance coefficients.

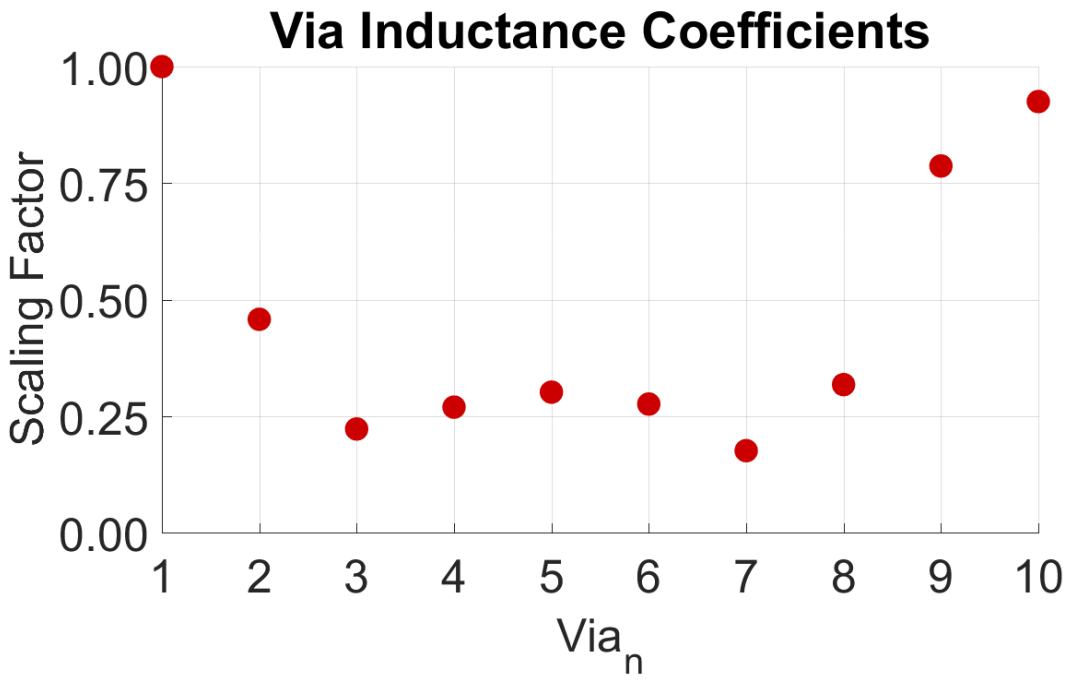

Figure 6.7: Normalized via inductance coefficients.

and S matrices identically to the previous version. The output S11 and S21 were plotted as before and are presented below in Figure 6.8. This behavior is much more reminiscent of the HFSS output seen in previous experiments and the resonances fall within the expected frequency range.

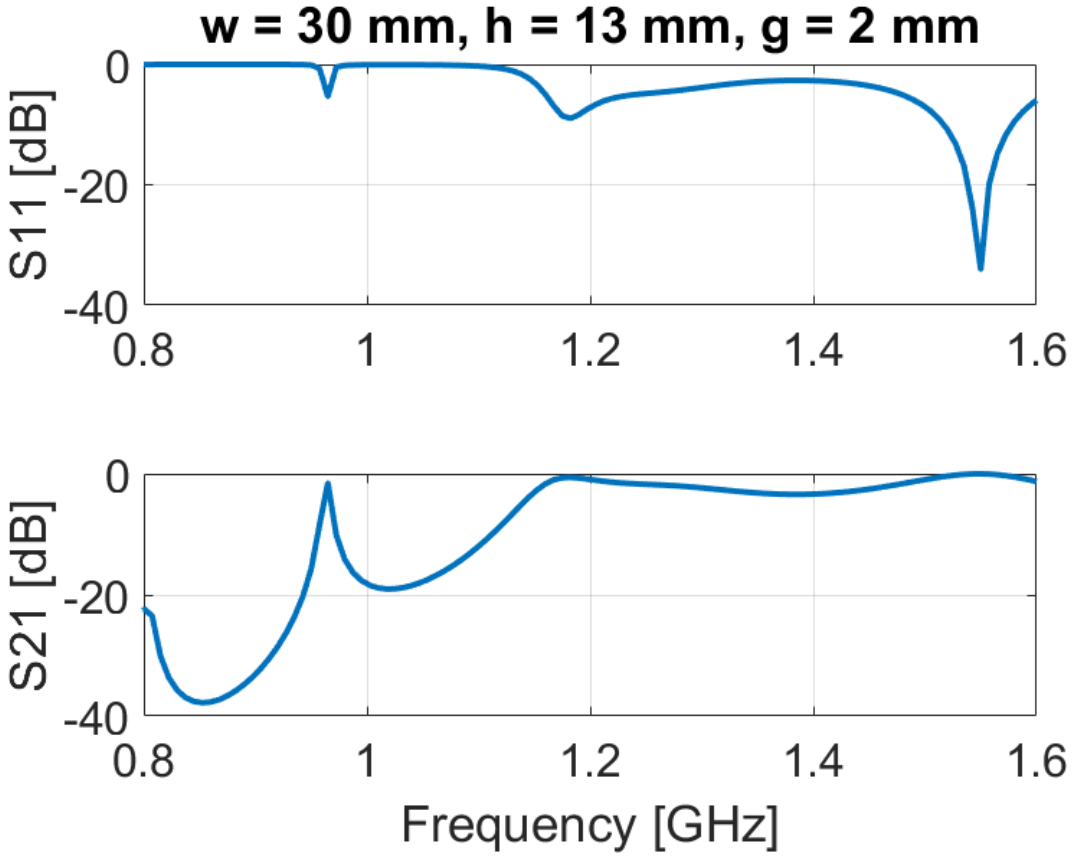

Figure 6.8: S-parameter output for Matlab model with modified scaling factors.

CHAPTER 7: CONCLUSIONS

7.1: EBG EFFICACY FOR RETROFIT COSITE INTERFERENCE REDUCTION

Significant progress has been made in the understanding and application of mushroom EBG structures for retrofit cosite interference between blade antennas. The stopband frequency is generally determined by the EBG patch width, substrate height, and dielectric constant of the material and the layering of the EBGs such as $Nz = 2$, $Nz = 3$ has negligible effect on stopband frequency. It was also determined that there is an upper limit to the number of EBG columns between two antennas before significant EBG-to-antenna coupling occurs, resulting in up to a 50 MHz upshift in low-end S11 in the L band case. If such allowance exists, an equivalent amount of coupling reduction over broad bandwidth can be achieved with a greater number of columns, *N*, and fewer layers, *Nz*. For multilayer EBGs some form of optimization should be done to fine tune the amount of coupling reduction over the entire band.

For the patch antenna case, the same effect on S11 was observed when the EBG became closer than about half of the free space wavelength at the lowest frequency of the active band. Even with this size restriction, coupling reduction in excess of 30 dB for the L1 band could be achieved while simultaneously reducing coupling by nearly 20 dB in the L2 band. It is suggested by this research that with proper tuning greater than 20 dB isolation improvement can be obtained across such a dual band configuration.

7.2: Current State of Analytical Model

The analytical model in Matlab shows band-stop behavior in the design band, although it is not yet a complete representation of the structure. Incorporating coefficients based on incident fields to the calculations of Z_C and Z_L led to simulation results more closely resembling the HFSS output. With this in mind, it seems that the proposed analysis method has the potential to reflect the behavior seen in HFSS given some refinement. Potential areas of improvement for the analytical model are discussed in the following section.

CHAPTER 8: FUTURE WORK

Much can be done to improve the current version of the analytical lumped circuit model of the EBG structure. Further comparison of the circuit model response to the response in HFSS should be investigated, including the effect of *w*, *g*, and *h* each have on overall performance. If the circuit model could encompass the EBG's proximity to the antennas and possibly even the antenna type by means of changing the nature of the incident field, a great deal of insight could be shed on the generalized behavior of these devices, potentially reducing design efforts by a significant amount. If the ultimate goal is a tool for design or optimization, then the scaling coefficients should be based on something other than fields simulated by another tool. In the case above, the intention of the preliminary circuit model was to analyze an existing design for which fields were known. Another area of future work would be to extend the model to two and three dimensions, as the reported analytical model only contains a single row and single layer. Observing and quantifying how incident fields and patch-to-patch coupling vary as rows and layers are added would be critical to the understanding and development of effective compact EBG structures such as the ones shown in Chapters 3, 4, and 5.

Future work for the EBG structures themselves should include investigations into non-uniform EBG design including tapering EBG patch sizes, using off-center vias, or even magnetic loading. Such designs could lead to more compact solutions for wideband problems.

REFERENCES

[1] D. F. Sievenpiper, *High-Impedance Electromagnetic Surfaces*, Ph.D. Dissertation, Electrical Engineering Dept., University of California, Los Angeles, 1999.

[2] D. Sievenpiper, L. Zhang, R. F. J. Broas, N. G. Alexopolus, and E. Yablonovitch, "High impedance electromagnetic surfaces with a forbidden frequency band," *IEEE Trans. Microwave Theory Tech.*, vol. 47, 2059–2074, 1999.

[3] F.-R. Yang, K.-P. Ma, Y. Qian, and T. Itoh, "A uniplanar compact photonic-bandgap (UC-PBG) structure and its applications for microwave circuits," *IEEE Trans. Microwave Theory Tech.*, vol. 47, no. 8, 1509–14, 1999.

[4] F.-R. Yang, *Novel Periodic Structures for Applications to Microwave Circuits*, Ph.D. Dissertation, Electrical Engineering Dept., University of California, Los Angeles, 1999.

[5] S. Clavijo, R. E. Díaz, and W. E. McKinzie, III, "Design Methodology for Sievenpiper High-Impedance Surfaces: An Artificial Magnetic Conductor for Positive Gain Electrically Small Antennas," *IEEE Trans. Antennas Propagat.*, vol. 51, no. 10, pp. 2678-2690, Oct. 2003.

[6] R. Coccioli, F. R. Yang, K. P. Ma, and T. Itoh, "Aperture-coupled patch antenna on UC-PBG substrate," *IEEE Trans. Microwave Theory Tech.*, vol. 47, pp. 2123–2130, Nov. 1999.

[7] R. Gonzalo, P. de Maagt, and M. Sorolla, “Enhanced patch-antenna performance by suppressing surface waves using photonic-bandgap substrates,” *IEEE Trans. Microwave Theory Tech*., vol. 47, no. 11, pp. 2131–2138, Nov 1999.

[8] R. F. J. Broas, D. F. Sievenpiper and E. Yablonovitch, “A high-impedance ground plane applied to a cell-phone handset geometry,” *IEEE Trans. Microwave Theory Tech.*, vol. 49, n0. 7, pp.1262–1265, July 2001.

[9] J.M. Bell and M.F. Iskander, “A low-profile Archimedean spiral antenna using an EBG ground plane,’’ *IEEE Antennas Wireless Propagat. Lett.*, Vol. 3, pp. 223-226, 2004.

[10] H. Nakano, K. Kikkawa, N. Kondo, Y. Iitsuka and J. Yamauchi, “Low-Profile Equiangular Spiral Antenna Backed by an EBG Reflector,’’ *IEEE Trans. Antennas Propagat.,* pp. 1309-1318, May 2009.

[11] R. C. Hansen, “Effects of a high-impedance screen on a dipole antenna,” *IEEE Antennas Wireless Propagat. Lett.*, vol. 1, pp. 46-49, 2002.

[12] F. Yang and Y. Rahmat-Samii, “Reflection phase characterizations of the EBG ground plane for low profile wire antenna applications,” *IEEE Trans. Antennas Propagat.,* vol. 51, no. 10, pp. 2691-2703, Oct. 2003.

[13] M. F. Abedin and M. Ali, “Effects of EBG Reflection Phase Profiles on the Input Impedance and Bandwidth of Ultra-thin Directional Dipoles,’’ *IEEE Trans. Antennas Propagat.,* vol. 53, no. 11, pp. 3664-3672, Nov. 2005.

[14] L. Akhoondzadeh-Asl, D. J. Kern, P. S. Hall, and D.H. Werner, *“*Wideband Dipoles on Electromagnetic Bandgap Ground Planes,’’ *IEEE Trans. Antennas Propagat.,* pp. 2426-2434, Sept. 2007.

[15] M. F. Abedin, M.Z. Azad, and M. Ali “WideBand Smaller Unit-Cell Planar EBG Structures and their Application,’’ *IEEE Trans. Antennas Propagat.,* March 2008, pp. 903-908.

[16] M.Z. Azad and M. Ali, “Novel Wideband Dipole Antenna on a Mushroom EBG Structure,’’ *IEEE Trans. Antennas Propagat.,* May 2008, pp. 1242-1250.

[17] S. Best and D. Hanna, “Design of a broadband dipole in close proximity to an EBG ground plane,’’ *IEEE Antennas and Propagation Magazine,* vol.50 pp. 52-64, Dec. 2008.

[18] N.H. Chamok, T. Anthony, S.J. Weiss, and M. Ali, “Ultra-Thin UHF Broadband Antenna on A Non-Uniform Aperiodic Metasurface,’’ *IEEE Antennas and Propagation Magazine,* vol. 57, pp. 167-180, April 2015.

[19] F. Yang and Y. Rahmat-Samii, "Microstrip antennas integrated with electromagnetic band-gap (EBG) structures: a low mutual coupling design for array applications," *IEEE Trans. Antennas Propagat.,* pp. 2936-2946, Oct. 2003.

[20] M. F. Abedin and M. Ali, “Effects of a Smaller Unit Cell Planar EBG Structure on the Mutual Coupling of a Printed Dipole Array,’’ *IEEE Antennas Wireless Propagat. Lett.,* vol. 4, pp. 274-276, August 2005.

[21] C-Y. Chiu, C-H. Cheng, R.D. Murch, and C.R. Rowell, "Reduction of mutual coupling between closely-packed antenna elements," *IEEE Trans. Antennas Propagat.,* pp. 1732-1738, June 2007.

[22] M.J. Al-Hassan, T.A. Denideni, and A.R. Sebak, "Mm-wave compact EBG structure for mutual coupling reduction applications," *IEEE Trans. Antennas Propagat.,*pp. 823-828, Feb. 2015.

[23] L. Qiu, F. Zhao, K. Xiao, S.-L. Chai, J.-J. Mao, "Transmit-receive isolation improvement of antenna arrays by using EBG structures," *IEEE Antennas and Wireless Propagation Letters,* vol. 11, 2012, pp. 93-96.

[24] E. R.-Iglesias, O. Q.-Teruel, and L. I.-Sanchez, "Planar soft surfaces and their application to mutual coupling reduction," *IEEE Trans. Antennas Propagat.,* pp. 3852-3859, Dec. 2009.

[25] D. Poduval, *Wideband Low Side Lobe Aperture Coupled Patch Phased Array Antennas,* M.S. Thesis, University of South Carolina, Columbia, South Carolina, 2017.

[26] D. Poduval and M. Ali, "Wideband Aperture Coupled Patch Array Antennas - High Gain, Low Side Lobe Design,'' *Journal Electromagnetics* (Submitted).

[27] D.M. Pozar and S.M. Duffy, "A dual-band circularly polarized aperture-coupled stacked microstrip antenna for global positioning satellite,'' *IEEE Trans. Antennas Propagat.,* pp. 1618-1625, Nov. 1997.

[28] M. Ali, A.T.M Sayem and V.K. Kunda, "A reconfigurable stacked microstrip patch antenna for satellite and terrestrial links,'' *IEEE Trans, Vehicular Technol.,* pp. 426-435, March 2007.